

Solid-State, Single-Ion-Conducting, Polymer Blend Electrolytes with Enhanced Li⁺ Conduction, Electrochemical Stability, and Limiting Current Density

Mengying Yang,^a Thomas H. Epps, III^{a,b,c,*}

^aDepartment of Materials Science & Engineering, University of Delaware, Newark, DE 19716, United States

^bDepartment of Chemical & Biomolecular Engineering, University of Delaware, Newark, DE 19716, United States

^cCenter for Research in Soft matter & Polymers (CRiSP), University of Delaware, Newark, DE 19716, United States

*Email: thepps@udel.edu

Abstract

The development of solid-state polymer electrolytes with high lithium conductivity is crucial to improve lithium-ion battery performance and ameliorate the safety challenges associated with current solvent-based electrolytes. Unfortunately, sluggish polymer segmental dynamics are known to constrain conductivity enhancements in solid-state polymer electrolyte systems, limiting overall performance. In this work, a glassy single-ion-conducting polymer, poly[lithium sulfonyl(trifluoromethane sulfonyl)imide methacrylate] (PLiMTFSI), was blended with a flexible polymer, poly(*oligo*-oxyethylene methyl ether methacrylate) (POEM), and the impact of PLiMTFSI molecular weight and ion concentration on the thermal and ion-conducting behavior of blend electrolytes was investigated. High ionic conductivities approaching 1×10^{-2} S/cm at 150 °C were realized in this polymer blend electrolyte system as a result of decoupling Li⁺ transport from polymer segmental dynamics. The decoupled ion transport was attributed to the packing frustration of the glassy PLiMTFSI – sufficient percolating free volume was generated to produce effective ion diffusion pathways. This decoupling was tunable as the ion transport could be altered from being closely coupled to the polymer segmental dynamics (Vogel–Tammann–Fulcher-like) to hopping (Arrhenius-like) by increasing the PLiMTFSI molecular weight and ion concentration. Moreover, the immobilized TFSI anion resulted in high Li⁺ selectivity (Li⁺ transference number = 0.9), high electrochemical stability (up to 4.7 V against Li⁺ / Li), and limiting current density of 1.8 mA/cm² (electrolyte thickness = 0.05 cm). These features suggest that this single-ion-conducting, polymer blend electrolyte might be a promising alternative to a benchmark system – salt-doped polyethylene oxide. Moreover, the above characteristics can support the battery operation at higher voltages using energy-dense Li metal anodes, with faster charging rates and enhanced energy/power densities. Overall, the results suggest that polymer chain packing frustration can be exploited to overcome the constraints of slow polymer segmental relaxations to achieve rapid and highly selective ion transport and enhanced performance in solid-state polymer electrolytes.

Introduction

Lithium-ion batteries (LiBs) are used in electric vehicles, consumer electronics products, and renewable energy storage devices,¹⁻³ and several desirable features for the next generation of these devices include faster charging rate, higher power/energy density, and enhanced safety.^{2,4-6} Current commercial liquid electrolytes, in which binary lithium salts and stabilizing additives are dissolved in flammable liquid solvents, offer high ionic conductivities ($\sim 10^{-3} - 10^{-2}$ S/cm at $-10 - 80$ °C) but low Li^+ transference numbers (t_{Li^+} , typically < 0.5) due to mobility of both the cation and anion.^{5,7} The low t_{Li^+} can lead to the formation of salt concentration gradients that accelerate Li dendrite formation and limit the charging/discharging rate, energy density, and cycling life of the battery.⁵ Moreover, many liquid electrolytes are susceptible to solvent leakage, thermal runaway, and eventual battery failure.⁸ The above-mentioned concerns can be substantially alleviated through the use of all-solid-state polymer electrolytes (SPEs) that provide both high t_{Li^+} and high ionic conductivity. Unfortunately, the inherent trade-off between transference number and conductivity remains a major challenge in the development of high-performance polymeric materials.⁵

Most current SPEs are based on polyethylene oxide (PEO).⁹ For example, PEO doped with Li bis(trifluoromethanesulfonyl)imide (LiTFSI) has reasonably high ionic conductivity ($\sim 10^{-3}$ S/cm at $60 - 100$ °C), low toxicity, and good thermal stability.^{5,10} The low glass transition temperature ($T_g \approx -60$ °C) of PEO facilitates fast segmental dynamics when the system is amorphous to support ion motion at temperatures well above T_g .¹¹ However, the high crystallinity of PEO below the melting temperature ($T_{m,\text{PEO}} \approx 62$ °C for $10 - 20$ kg/mol) leads to a significant reduction in conductivity near room temperature.¹² There have been numerous studies focused on disrupting crystallinity in PEO using PEO-grafted polymethacrylates^{13,14} and PEO-based copolymers.¹⁵⁻²⁴ For instance, poly(*oligo*-oxyethylene methyl ether methacrylate) (POEM), with its ether-oxygen side chains, has shown promise in terms of significantly improved room-temperature conductivity vs. analogous salt-doped PEO systems when the appropriate side-chain lengths are employed.^{13,15} Other approaches also have been developed to decrease the crystallinity of PEO, including nanoparticle addition,²⁵⁻²⁷ polymer blending,^{26,28} and crosslinking.²⁹⁻³¹ Additionally, small-molecule plasticization³²⁻³⁶ and low- T_g segment introduction³⁷⁻⁴⁰ have been shown to accelerate segmental relaxation, and polymer architecture modification can effectively alter the Li^+ -polymer coordination^{14,41-44} and/or the Li^+ solvation-site connectivity.^{14,45-47} Although improved overall conductivities have been achieved, the significant anion motion in these PEO-based electrolytes results in low t_{Li^+} (≈ 0.2),^{48,49} and therefore relatively modest Li^+ conductivities ($\sim 10^{-4}$ S/cm at $60 - 100$ °C).

Apart from modest Li^+ conductivities in PEO-based electrolytes, low t_{Li^+} also limit electrochemical windows in these systems by accelerating the irreversible anion oxidation or reduction near the electrode, and therefore decreasing the electrochemical stabilities of SPEs.⁵⁰ The benchmark LiTFSI-doped PEO (PEO/LiTFSI) system has a low electrochemical stability (~ 3.5 V vs. ~ 4.2 V for liquid electrolytes against Li^+ / Li),⁵¹⁻⁵³ not suitable for using energy-dense anodes such as Li metal in batteries. The widely adopted strategies for improving electrochemical stabilities of PEO-based SPEs include introducing another high voltage-resistant SPE⁵⁴ or inorganic component^{55,56} and constructing kinetically stable interfaces at the electrode surface.⁵⁷ End-group modification also has shown promise in widening the electrochemical stability windows.⁵⁸ Although improved electrochemical stabilities have been realized ($\sim 4.0 - 4.3$ V against Li^+ / Li), decreased overall conductivities are seen in some systems in comparison to the benchmark PEO/LiTFSI system.^{54,58}

SPEs with low t_{Li^+} also limit relative improvements in another important parameter, the limiting current density.^{59,60} The limiting current density dictates the largest sustainable current density that can be passed through the electrolytes,⁶⁰ with higher values indicative of more rapid charging of the battery. In SPEs with significant anion motion (low t_{Li^+}), the gradual buildup of a salt concentration polarization leads to Li^+ depletion at the cathode, and therefore lower limiting current densities.^{59,60} It has been reported that the variation in Li^+ solvation environment can lead to improved limiting current densities in comparison to PEO/LiTFSI by 2.8 fold, but at a cost of almost an order-of-magnitude decrease in overall conductivities.⁵²

The challenges associated with low t_{Li^+} in polymers can be largely addressed through immobilization of the anions, i.e., rendering the electrolytes as single-ion-conducting (SIC). SIC polymers typically have relatively high T_g s (> 60 °C),^{61,62} resulting in significantly limited segmental relaxation to support rapid Li^+ transport in comparison to PEO-based electrolytes ($T_g \approx -60$ °C). Moreover, the inherently strong electrostatic interactions between the anion and Li^+ lead to insufficient free Li^+ concentrations, thereby reducing conductivities. Both features lead to low conductivities in SIC homopolymers ($\sim 10^{-8} - 10^{-6}$ S/cm at 200 °C).^{61,62} To date, various approaches have been adopted to enhance the conductivities of solid-state SIC polymer electrolytes, for instance, copolymerizing⁶³⁻⁶⁷ or blending^{68,69} with a low- T_g , ion-solvating polymer, such as PEO ($T_g \approx -60$ °C),¹¹ PEO-derivative, or polyvinylidene fluoride ($T_g \approx -35$ °C).⁷⁰ However, the conductivities of all-solid-state SIC polymer electrolytes have been relatively modest, plateauing at $\sim 10^{-5} - 10^{-4}$ S/cm at 90 – 110 °C.^{61,64,66} The limited conductivities are attributed to the inherent anticorrelation between fast segmental relaxation and sufficient free Li^+ .⁷¹ Promising conductivities ($\sim 10^{-3}$ S/cm) that may support many battery applications typically are only achieved in solvent-plasticized systems – at the potential cost of battery safety and electrochemical stability.⁷²⁻⁷⁵ The above-mentioned systems consist of either low ion concentrations (molar ratio between coordinating groups and ions $\approx 20:1$) and/or low ($\sim 4 - 8$ kg/mol) to intermediate ($\sim 10 - 30$ kg/mol) molecular-weight polymer(s), rendering these systems ‘soft’ and making them prone to pack space relatively tightly/efficiently.^{76,77} Thus, ion diffusion in these soft systems is possible only when polymer segmental relaxation occurs.⁷⁷ Although restricted anion motion (high t_{Li^+}) typically is expected to improve electrochemical stabilities (4.6 – 7.0 V)^{78,79} and limiting current densities (seldom reported for SIC SPEs),^{52,59,60,75} one conundrum in these systems is that fast segmental dynamics requires relatively low Li^+ concentration to reduce T_g suppression,^{71,80} whereas sufficient amount of free Li^+ is crucial to enhance conductivities.⁷¹ This inherent anticorrelation remains the major challenge in the development of solid-state SIC systems that simultaneously exhibit high conductivities, Li^+ selectivities, electrochemical stabilities, and limiting current densities.

There have been a few successful reports on decoupling Li^+ diffusion from segmental dynamics to address this inherent anticorrelation in SIC polymer electrolytes. For instance, in the copolymer system consisting of (ethylene glycol) methyl ether acrylate and lithium 3-[(trifluoromethane) sulfonamidodisulfonyl]propyl methacrylate, the percolating and locally dynamic ionic aggregates supported Li^+ transport.⁸¹ The highest conductivities ($\sim 10^{-3}$ S/cm at 150 °C) in this system were comparable to PEO/LiTFSI.⁸¹ Other reports have focused on zwitterionic polymer-based electrolytes in which Li^+ hopped within the liquid-like electrolytes.⁸²⁻⁸⁴ The overall conductivities ($\sim 10^{-4} - 10^{-3}$ S/cm at 80 – 110 °C) were comparable to PEO/LiTFSI with improved Li^+ selectivities ($t_{\text{Li}^+} = 0.6 - 0.8$)⁸²⁻⁸⁴ and electrochemical stabilities (3.8 V against Li^+ / Li).⁸²

Apart from Li^+ diffusion through ionically dense environments, percolating free volume in the polymers can be used as efficient transport pathways.⁸⁵⁻⁸⁷ This unstructured free volume is

largely present in polymers that are inherently packing frustrated,^{85,86,88} such as poly(ionic liquids) with rigid backbone and/or pendent groups. The significantly frustrated (inefficient) chain packing resulted in ~ 6 orders of magnitude conductivity enhancement (from $\sim 10^{-15}$ S/cm to $\sim 10^{-9}$ S/cm) at T_g (≈ -20 °C) vs. analogous SPEs, in which the ion diffusion was closely coupled with segmental relaxation.⁸⁹ Moreover, polymers with higher molecular weights exhibited more pronounced decoupling and conductivity enhancement.⁹⁰ This phenomenon was attributed to longer chains imposing more constraints on molecular movement due to chain connectivity.⁹⁰ Taken together, the overall conductivity trends in the aforementioned SIC polymer electrolytes suggest that the ability to decouple the ion transport from polymer segmental relaxation may be an effective approach to simultaneously realize high conductivities and high Li^+ selectivities.

Herein, a glassy SIC homopolymer with highly delocalized anion was blended with a flexible PEO-derivative, and the blend electrolyte's thermal and ion-conductive properties were investigated as a function of SIC polymer molecular weight and ion concentration. The rigid SIC homopolymer was intrinsically packing frustrated, and the significant unstructured percolating free volume likely generated through its incorporation was able to support fast and efficient Li^+ transport. The ether oxygen/ Li^+ interaction readily dissociated the Li^+ from its anion, providing sufficient free Li^+ to contribute to ionic conductivities. The immobilized anion led to high Li^+ selectivities, electrochemical stabilities, and limiting current densities. Moreover, the conducting behavior of this polymer blend electrolyte could be readily linked to polymer molecular weight, T_g , and fragility, providing a recipe to improve conductivities in full SPEs. Taken together, this SIC polymer blend electrolyte system with easily tailorable compositions simultaneously exhibited superior ionic conductivities up to $\approx 7 \times 10^{-3}$ S/cm at 150 °C, Li^+ selectivities of $t_{\text{Li}^+} = 0.9$, electrochemical stabilities up to 4.7 V against Li^+ / Li , and limiting current densities of 1.8 mA/cm² (electrolyte thickness = 0.05 cm), outperforming the benchmark PEO/LiTFSI system in terms of overall metrics.

Experimental Section

Chemicals. *Oligo*-oxyethylene methyl ether methacrylate (OEM, > 99%, stabilized, average molar mass = 500 g/mol, Sigma-Aldrich, USA) was purified by passage through a basic aluminum oxide column. Lithium sulfonyl(trifluoromethane sulfonyl)imide methacrylate (LiMTFSI, 99%, stabilized, Specific Polymers, France), copper bromide [Cu(II)Br, 98%, Acros Organics, USA], tris(2-pyridylmethyl)amine (TPMA, 98%, Sigma-Aldrich, USA), ethyl 2-bromoisobutyrate (EBib, 98%, Sigma-Aldrich, USA), tin(II) 2-ethylhexanoate [Sn(Oct)₂, 92.5 – 100.0%, Sigma-Aldrich, USA], anisole (> 99%, Fisher Scientific, USA), dimethylformamide (DMF, Fisher Scientific, USA), diethyl ether (Fisher Scientific, USA), petroleum ether (Fisher Scientific, USA), acetone (Optima, Fisher Scientific, USA), acetone-d₆ (with 0.03 v/v % tetramethylsilane, 99.9 atom% D, Thermo Scientific, USA), chloroform-d (with 0.02 – 0.04 v/v % tetramethylsilane, 99.8+ atom% D, Thermo Scientific, USA), and lithium bromide (LiBr, $\geq 99\%$, Sigma-Aldrich, USA) were used as received.

Synthesis of Poly(lithium sulfonyl(trifluoromethane sulfonyl)imide methacrylate) (PLiMTFSI) and Poly(*oligo*-oxyethylene methyl ether methacrylate) (POEM). PLiMTFSI and POEM homopolymers were synthesized by Activators ReGenerated by Electron Transfer Atom Transfer Radical Polymerization (ARGET ATRP) under similar protocols, as described in the following example. In a typical PLiMTFSI polymerization, Cu(II)Br (0.0025 mmol), TPMA (0.025 mmol), and DMF were mixed and stirred for 2 h to ensure full complexation between the copper and the ligand. Then, the catalyst solution was combined with LiMTFSI (11.5 mmol), EBib

(0.025 mmol), and DMF in a three-neck, round-bottom Schlenk flask and was degassed *via* three freeze-pump-thaw cycles. Separately, Sn(Oct)₂ (0.025 mmol) and anisole were mixed and sparged with argon gas under stirring for 30 min. To initiate the reaction, the reducing agent [Sn(Oct)₂] solution was added to the reaction flask, which was placed in a thermostatic oil bath at 90 °C. The reaction conversion was monitored by Proton Nuclear Magnetic Resonance (¹H NMR, Bruker AV600III) spectroscopy with acetone-d₆ (with 0.03 v/v % tetramethylsilane) as a solvent. The reaction was allowed to proceed for 17 h when the desired conversion (~ 60%) was achieved. Then, the reaction was quenched by immersing the flask in liquid nitrogen, after which the flask was opened to air. Next, the reaction solution was precipitated into a mixture of petroleum ether and diethyl ether (1:1 by volume), and the polymer was separated from the supernatant *via* centrifugation. The polymer was redissolved in acetone and reprecipitated into petroleum ether/diethyl ether mixture until LiMTFSI monomer was not visible in the ¹H NMR spectrum of the purified polymer. Typically, four precipitations were required to sufficiently remove unreacted LiMTFSI. The polymer then was sealed in a drying chamber and dried under dynamic vacuum at ambient temperature until the Schlenk line baseline pressure was reached; this process typically took ~ 10 h. To ensure that any residual solvent and moisture were removed, the temperature was slowly increased to 150 °C in 10 °C increments. After the Schlenk line baseline pressure was reached (~ 4 h), the polymer was dried at 150 °C under dynamic vacuum for 48 h prior to storage in a -4 °C freezer in an argon-filled glovebox.

Blend Electrolyte Film Fabrication. PLiMTFSI and POEM stock solutions were prepared in an argon-filled glove box by dissolving each material separately in anhydrous DMF at ~ 10 wt% and then stirring for 24 h. Next, the appropriate PLiMTFSI and POEM stock solutions were mixed at varying gravimetric ratios and stirred for another 48 h. The Li⁺ concentration was quantified in all samples as [EO]:[Li] (denoted as *r*), which represents the molar ratio of ethylene oxide monomer segments in the side chains of POEM to Li⁺ in PLiMTFSI. The composition of each blend electrolyte was denoted as ‘PLiMTFSI – X / POEM, *r*,’ in which X represents the PLiMTFSI number-average molecular weight *M_n* (*M_{n,PLiMTFSI}*) in kg/mol as determined by size exclusion chromatography.

Next, the blend electrolyte solution was taken out of the glovebox and drop-casted onto a Teflon o-ring mold to form a uniform film with 0.05 cm thickness (*L*) and 0.32 cm² area (*A*). The majority of the DMF was slowly evaporated under an inert atmosphere to ensure uniform thickness and prevent bubble formation in the film. After the film was formed, it was sealed in a drying chamber and dried under dynamic vacuum at ambient temperature until the Schlenk line baseline pressure was reached (~ 20 h). To ensure residual solvent and moisture were removed, the temperature was slowly increased to 150 °C in 10 °C increments. After the Schlenk line baseline pressure was reached (~ 6 h), the electrolytes were dried at 150 °C under dynamic vacuum for 48 h. The dried electrolyte films were stored in an argon-filled glovebox prior to characterization.

Size Exclusion Chromatography (SEC). SEC was performed on an HLC-8420 EcoSEC Elite Gel Permeation Chromatography instrument, with 0.1 vol% LiBr in DMF as the eluent at 25 °C (0.8 mL/min) and two PL aquagel-OH Mixed-H (8μm, 50×7.5 mm) columns. A calibration curve was constructed using narrow-dispersity poly(methyl methacrylate) standards (885 – 2,210,000 g/mol, purchased from Agilent Technologies, USA). Samples were prepared by dissolving ~ 5 mg polymer in ~ 5 mL SEC solvent. All samples were left at ambient temperature for 24 h to ensure complete dissolution and then filtered using 0.1-μm PTFE filters prior to measurement.

Thermogravimetric Analysis (TGA). Neat PLiMTFSI and neat POEM samples (2-3 mg) were loaded into 100- μ L platinum pans and heated under continuous N₂ flow (50 mL/min). Measurements were conducted on a TA Instruments Discovery TGA instrument. Samples were heated at 20 °C/min to 115 °C, annealed at 115 °C for 5 min to remove any residual water, cooled at 20 °C/min to 50 °C, held at 50 °C for 1 min, and heated at 15 °C/min to 600 °C.

Differential Scanning Calorimetry (DSC). Bulk electrolyte samples (~ 8 mg) were hermetically sealed in 40- μ L aluminum pans in an argon-filled glovebox. Measurements were conducted on a TA Instruments Discovery DSC instrument with an RCS90 cooling accessory. Baseline and cell constant calibrations were performed using sapphire disks and an indium standard, respectively. Three heating/cooling cycles at 10 °C/min ramp rate were performed under an N₂ environment within appropriate temperature windows: 0 – 200 °C for neat PLiMTFSI; -80 – 150 °C for neat POEM, -80 – 120 °C for PLiMTFSI – 7 / POEM blends; -80 – 150 °C for PLiMTFSI – 16 / POEM blends; -80 – 160 °C for PLiMTFSI – 25 / POEM blends; -80 – 190 °C for PLiMTFSI – 52 / POEM and PLiMTFSI – 105 / POEM blends. The reported T_g values were determined from the midpoints of the inflections in the third heating traces. The second and third heating traces were compared to ensure reproducibility upon heating.

Dynamic Mechanical Analysis (DMA). DMA was carried out using an ARES-G2 strain-control rheometer (TA Instruments). Samples were hot-pressed at 30 °C (for neat POEM), 170 °C (for neat PLiMTFSI – 52), and 60 °C (for PLiMTFSI – 52 / POEM, $r = 10:1$) for 5 min in the rheometer under an axial force of 0.2-1.0 N before shear measurements to improve contact between the polymer and the plates. For the neat POEM sample, a cone and plate geometry (with a 25-mm diameter and a 0.0998-rad cone angle) was used due to the liquid-like nature of the sample.⁹¹ For neat PLiMTFSI – 52 and PLiMTFSI – 52 / POEM, $r = 10:1$ samples, 8-mm-diameter parallel plates were used. An approximately 0.4 mm thick sample was placed between the cone and plate or between the two plates in a closed oven under an N₂ environment. The sample was exposed to ambient atmosphere for less than 1 min when loading into the rheometer, and thus, moisture uptake was minimized.⁹² Isothermal frequency sweeps were conducted at 5 °C temperature increments and at appropriate strain amplitudes, which were varied to keep sample behavior within the linear viscoelastic region⁹³ (200 – 220% for neat POEM, 0.1 – 0.5% for neat PLiMTFSI – 52, and 0.5 – 0.8% for PLiMTFSI – 52 / POEM, $r = 10:1$). The temperature range was 30 – 150 °C, which is the same as the conductivity measurement temperature range and is of interest for practical battery operation.

Alternating Current (AC) Impedance Spectroscopy. Ionic conductivities were measured using a Princeton Applied Research PARSTAT 2273 frequency response analyzer with a homemade test cell mounted on a Linkam HFS91 CAP stage, under vacuum in a standalone chamber. The homemade test cell consisted of two stainless steel electrodes and two aluminum blocking electrodes with a Teflon o-ring spacer in the middle to prevent short-circuiting. The blend electrolyte film was sandwiched between the aluminum electrodes, and the cell was assembled in an argon-filled glovebox. Prior to the ionic conductivity measurement, all samples were annealed at 60 °C for 3 h in the sealed test cell to ensure good contact with the aluminum electrodes, then the samples were cooled to 25 °C and held at that temperature for 1 h. The ionic conductivities were measured on heating between 30 °C and 150 °C in 10 °C increments. At each temperature, two impedance measurements were taken after annealing for 5 min and 8 min, respectively. The reported ionic conductivities at each temperature were the average of the ionic conductivities calculated for the two impedance measurements at that respective temperature. The differences between the two calculated ionic conductivities at a given temperature were generally on the order

of 1% or less, indicated that the cells were stable and that consistent ionic conductivity results were obtained during the process. The AC frequency range was 0.1 Hz – 1 MHz, and the voltage amplitude was 10 mV. The choice of a small voltage amplitude ensured a linear region of behavior to simplify the analysis. The bulk resistance (R_{bulk}) of the blend electrolyte was determined from the high-frequency plateau in the real impedance data,^{92,94} and the ionic conductivity (σ) was calculated using eq (1),

$$\sigma = \frac{L}{R_{bulk} \times A}. \quad (1)$$

AC impedance spectroscopy was also conducted on three replicate lithium – lithium symmetrical cells with PLiMTFSI – 52 / POEM, $r = 10:1$ electrolyte to ensure consistent conductivity results were obtained between using blocking and non-blocking electrodes. The lithium foil (battery grade, 0.01 cm thickness, 7.1 cm width, lithium content $\geq 99.95\%$, China Energy Lithium Co., Ltd, China) was used as received. Lithium foil electrodes with 0.95 cm diameter (3/8 inches) were prepared using a hollow punch with a 3/8-inch (0.95 cm) cutting head (Mayhew Steel Products, Inc., USA) in an argon-filled glovebox.

Potentiostatic Polarization. A lithium transference number (t_{Li^+}) was measured by potentiostatic polarization and AC impedance spectroscopy under vacuum using a Princeton Applied Research PARSTAT 2273 frequency response analyzer in a lithium – lithium symmetric cell that was mounted on a Linkam HFS91 CAP stage. The cell consisted of two stainless steel electrodes and two lithium electrodes with a Teflon o-ring spacer in the middle. The polymer blend electrolyte film (PLiMTFSI – 52 / POEM, $r = 10:1$) was sandwiched between the lithium electrodes, and the cell was assembled in an argon-filled glovebox. Three replicate lithium – lithium symmetric cells were made as described above. Prior to any electrochemical measurement, the cell was heated up to 60 °C and allowed to equilibrate for 3 h. Then, an AC impedance spectroscopy measurement was conducted prior to the potentiostatic polarization, and the initial impedance was recorded as a function of frequency. After this measurement, the cell was polarized with a potential of 10 mV (a small polarization voltage was chosen to avoid any significant electrochemical reactions that might affect the final results). For the first 0.98 s, a sampling rate of 1 ms⁻¹ was used to measure the initial current.⁹⁵ This sufficiently fast sampling rate ensured accurate determination of the initial current.⁹⁵ The current was closely monitored during the polarization process in 20-s time intervals, and the potential was applied for 6 h, at which point a steady-state current was reached. An AC impedance spectroscopy measurement then was performed again to extract the steady-state impedance, with an AC frequency range of 0.1 Hz – 1 MHz and a voltage amplitude of 10 mV. t_{Li^+} was determined using the Bruce-Vincent method (eq 2),⁹⁶

$$t_{Li^+} = \frac{I_{SS}(\Delta V - I_0 R_0)}{I_0(\Delta V - I_{SS} R_{SS})}, \quad (2)$$

in which I_{SS} and I_0 are the steady-state and initial current, respectively, ΔV is the polarization voltage, and R_{SS} and R_0 are the steady-state and initial interfacial impedance, respectively. The interfacial impedance was taken as the difference between the values of the minima at the bounds of the low-frequency semicircle in a Nyquist plot.⁴⁹ The reported t_{Li^+} value was taken as the average of the data obtained from the four cells.

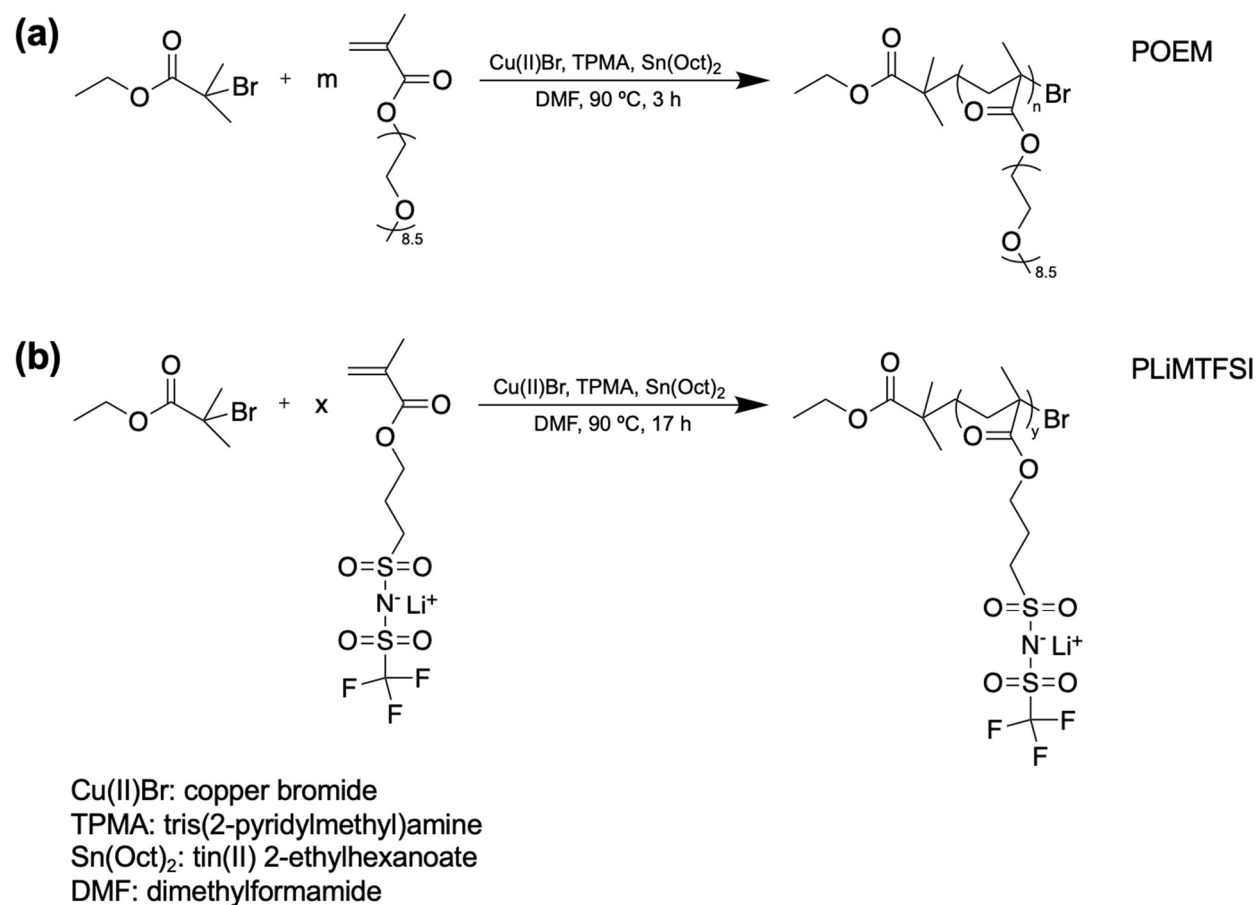
Chronopotentiometry. A limiting current density was determined through a chronopotentiometry method under vacuum using a Princeton Applied Research PARSTAT 2273 frequency response analyzer in a lithium – lithium symmetric cell that was mounted on a Linkam HFS91 CAP stage. The cell consisted of two stainless steel electrodes and two lithium electrodes with a Teflon o-ring spacer in the middle. The polymer blend electrolyte film (PLiMTFSI – 52 / POEM, $r = 10:1$) was sandwiched between the lithium electrodes, and the cell was assembled in an argon-filled glovebox. Three replicate lithium – lithium symmetric cells were made as described above. Prior to the measurement, the cell was heated up to 60 °C and allowed to equilibrate for 3 h. All experiments were performed at 60 °C under increasing current densities from 0.8 mA/cm² to 1.9 mA/cm². The voltage was closely monitored during the measurements in 6-s time intervals. The limiting current density was determined to be the highest current density at which a steady-state potential was reached, which typically took 1.5 h.

Linear Sweep Voltammetry. Electrochemical stability was determined by linear sweep voltammetry under vacuum using a Princeton Applied Research PARSTAT 2273 frequency response analyzer in a lithium – stainless steel cell that was mounted on a Linkam HFS91 CAP stage. The polymer blend electrolyte film (PLiMTFSI – 52 / POEM, $r = 10:1$) was sandwiched between the stainless steel electrode and the lithium electrode, with a Teflon o-ring in the middle of the two electrodes, then backed with another stainless steel electrode. The cell was assembled in an argon-filled glovebox. Three replicate lithium – stainless steel cells were made as described above. The experiment was performed at 60 °C under increasing cell potentials from 1.0 V to 6.0 V at a scan rate of 0.1 mV/s, and the current was closely monitored during the measurement.

Results and Discussion

Enhanced Li⁺ conductivities are realized as Li⁺ hops through free volume voids.

To investigate the effect of the degree of packing frustration on the ion conduction behavior, POEM and a series of SIC homopolymers – PLiMTFSI – were synthesized *via* ATRP (**Scheme 1**; molecular characterization details are located in **Figures S1 – S3** and **Table S1**; thermal stability characterization details are located in **Figure S4** and **Figure S5**; glass transition characterization details are located in **Figures S6 – S11**). The M_n of the POEM was 5.9 kg/mol, and the $M_{n,PLiMTFSI}$ ranged from 7.0 to 105.7 kg/mol. PLiMTFSI and POEM were blended at various ion concentrations at $5:1 < r < 30:1$. PLiMTFSI and POEM were miscible in all the polymer blends, as indicated by a single T_g measured using DSC (see **Figures S7 – S11**, **Table S2**, and the associated text). The rigidity of PLiMTFSI and POEM was evaluated through DMA by measuring the shear storage modulus, which can be used to describe the rigidity of a material,⁹⁷ and PLiMTFSI has ~ 7 order-of-magnitude higher rigidity than POEM (see **Figure S12**). In comparison to PEO/LiTFSI,⁹² the shear storage modulus of PLiMTFSI – 52 / POEM, $r = 10:1$ electrolyte (**Figure S13**) has an at least ~ 2 order-of-magnitude enhancement, owing to the PLiMTFSI incorporation.



Scheme 1. Synthesis scheme for (a) POEM and (b) PLiMTFSI.

The temperature-dependent ionic conductivities were determined by AC impedance spectroscopy using aluminum blocking electrodes, see **Figure 1**. The conductivity results obtained using lithium non-blocking electrodes with PLiMTFSI – 52 / POEM, $r = 10:1$ electrolyte are shown in **Figure S14** and **Table S3**. The ionic conductivities obtained using blocking and non-blocking electrodes were in relatively good agreement.⁸² The data points were fit with either dashed or solid lines using the following delineations. The dashed lines were applied to conductivity results that were well described ($R^2 \geq 0.99$) by the Vogel–Tammann–Fulcher (VTF) equation (eq 3),⁷¹

$$\sigma = \sigma_0 \exp \left[\frac{-E_a}{R(T-T_0)} \right], \quad (3)$$

in which E_a is the pseudo activation energy associated with polymer segmental dynamics, R is the ideal gas constant, T is the absolute temperature in Kelvin, and T_0 is the ideal T_g at which the free volume or configurational entropy becomes zero.⁷¹ Herein, T_0 was chosen to be 50 K below T_g of the blend electrolyte ($T_{g,blend}$), which is common for polyether-containing systems.⁹⁸⁻¹⁰² The VTF-type behavior suggested that ion-polymer motion was cooperative and that ion transport was

closely coupled to the polymer segmental relaxation.⁷¹ The solid lines were applied to conductivity results that were well described ($R^2 \geq 0.99$) by the Arrhenius equation (eq 4),¹⁰³

$$\sigma = \sigma_0 \exp\left(\frac{-E_a}{RT}\right), \quad (4)$$

in which σ_0 is the ionic conductivity at infinitely high temperature, and E_a is the pseudo activation energy associated with ion hopping.¹⁰³ The Arrhenius-type behavior implied that ion transport was likely a thermally activated process as ions hopped from one available site to another.¹⁰³ This type of ion transport was considered decoupled from polymer segmental relaxation.^{86,88-90,103,104}

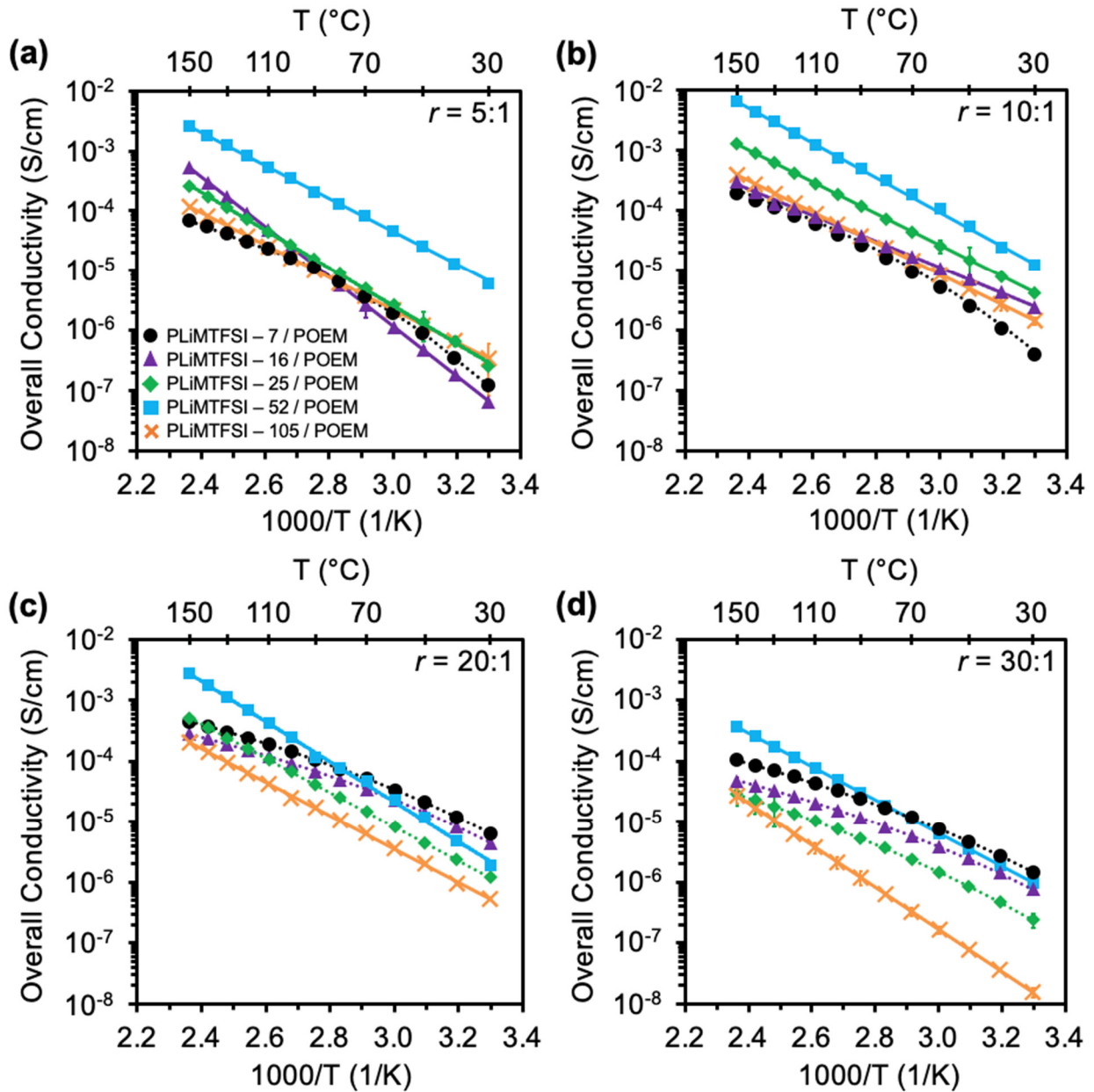


Figure 1. Overall ionic conductivities (data points) and fits (lines) as a function of $1000/T$ for blend electrolytes at (a) $r = 5:1$, (b) $r = 10:1$, (c) $r = 20:1$, and (d) $r = 30:1$. VTF-like fits to conductivities are shown by dashed lines; Arrhenius-like fits to conductivities are shown by solid lines. The error bars (most of which are smaller than the data points) represent the standard deviations from averaging the 5-min and 8-min impedance measurements.

At high ion concentrations ($r = 5:1$ and $10:1$, **Figure 1a** and **Figure 1b**), all of the blends displayed Arrhenius-like ion diffusion (shown by solid lines) except PLiMTFSI – 7 / POEM, which exhibited VTF-like ion transport (shown by dashed lines). This prevalence of decoupled ion transport was likely a result of the free volume that comes from the packing frustration of both

glassy PLiMTFSI, as well as transient TFSI⁻ – Li⁺ – EO crosslinks.¹⁰⁵⁻¹⁰⁷ This unstructured free volume can yield interconnected voids with various sizes and distributions as transport pathways,¹⁰⁸ through which Li⁺ can hop with enough thermal energy. Herein, the conductivities increased by ~ 2 orders of magnitude (from ~ 10⁻⁴ S/cm to ~ 10⁻² S/cm at 150 °C) as $M_{n,PLiMTFSI}$ increased from 16 kg/mol to 52 kg/mol. However, a drop in conductivities occurred when $M_{n,PLiMTFSI}$ was raised to 105 kg/mol.

For blend electrolytes with low ion concentrations ($r = 20:1$ and $30:1$, **Figure 1c** and **Figure 1d**), the majority of blend systems displayed VTF-like ion diffusion behavior (shown by dashed lines), and only PLiMTFSI – 52 / POEM and PLiMTFSI – 105 / POEM systems exhibited Arrhenius-like ion transport (shown by solid lines). This crossover between VTF- and Arrhenius-type behavior at higher molecular weights likely occurred because longer chains impose more constraints on molecular movement due to chain connectivity, resulting in more frustrated chain packing.⁹⁰ Additionally, the transient TFSI⁻ – Li⁺ – EO crosslinks were not as prevalent at the lower salt concentrations because there was sufficient coordination capacity available through the POEM.¹⁰⁵⁻¹⁰⁷ Taken together, these composition-dependent conductivity results suggest that variations in glassy polymer chain length and the ion concentration can be used to tune the degree of packing frustration, and therefore the free volume within the materials.

This ion transport mechanism transition also is illustrated in **Figure 2a** and **Figure 2b**, by plotting the conductivity as a function of $M_{n,PLiMTFSI}$. For electrolytes with high ion concentrations ($r = 5:1$ and $10:1$), the conductivities initially improved with increasing $M_{n,PLiMTFSI}$ (from 7 kg/mol to 52 kg/mol) then dropped when $M_{n,PLiMTFSI}$ was further raised to 105 kg/mol. A slight deviation of this trend was noted in $r = 5:1$ at 60 °C (a drop in conductivities occurred as $M_{n,PLiMTFSI}$ increased from 7 kg/mol to 16 kg/mol), which might be largely correlated with the local transport environment difference at 60 °C vs. 90 °C due to the dynamic character of the free volume voids.^{109,110} For blend electrolytes with low ion concentrations ($r = 20:1$ and $30:1$), the conductivities at lower molecular weights dropped with increasing $M_{n,PLiMTFSI}$ (from 7 kg/mol to 25 kg/mol), likely due to an increase in $T_{g,blend}$ across the regime in which ion diffusion was dependent on polymer segmental relaxation. Then, the conductivities rose as $M_{n,PLiMTFSI}$ increased to 52 kg/mol, likely because the ion transport mechanism transitioned from ion/polymer cooperative motion to ion hopping (described by the Arrhenius relationship in **Figure 1c** and **Figure 1d**), the latter of which is suggested to proceed faster than the former.^{90,104} Finally, the conductivities decreased when $M_{n,PLiMTFSI}$ increased to 105 kg/mol. The nonmonotonic trend of conductivity vs. $M_{n,PLiMTFSI}$ implies that molecular weight is not the sole contributor to the polymer packing frustration. Apart from the molecular weight,^{111,112} there are other factors impacting the efficiency of polymer chain packing space and the corresponding free volume, such as the dispersity,¹¹³ the backbone rigidity,^{114,115} the ‘relative’ rigidity of the side group(s) vs. the backbone,¹¹⁶ the molecule symmetry,¹¹⁷ end-group chemistry,^{118,119} and inter- / intra-molecular interactions.¹²⁰⁻¹²² These factors are typically cross-correlated in polymer systems, and a detailed deconvolution is beyond the scope of this work.

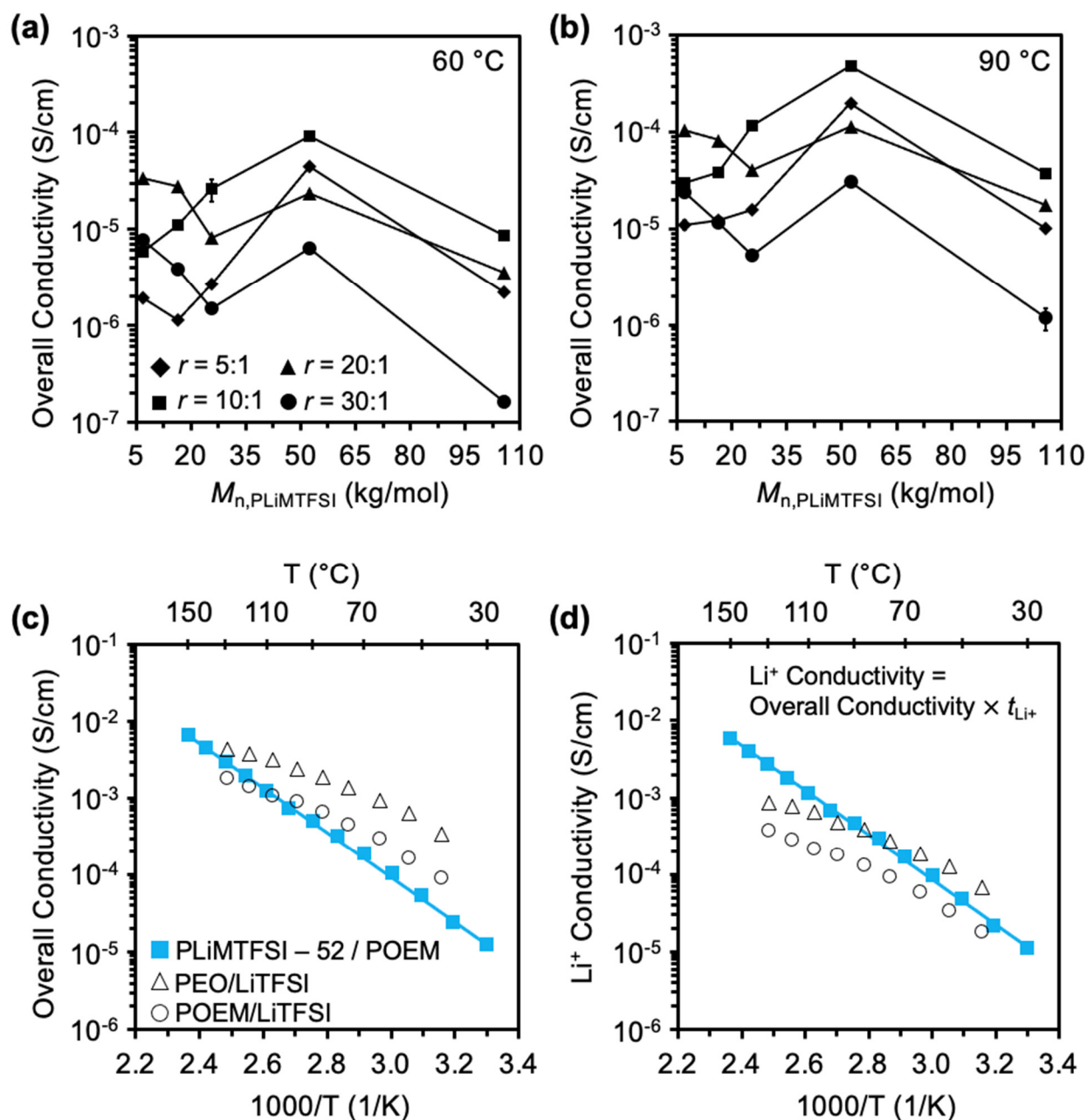


Figure 2. Overall ionic conductivities as a function of r and $M_{n,PLiMTFSI}$ at (a) 60 °C and (b) 90 °C. The lines between data points are to guide the eye. Comparison of temperature-dependent (c) overall conductivities and (d) Li^+ conductivities for PLiMTFSI – 52 / POEM, $r = 10:1$ (blue filled squares, fit to the Arrhenius equation shown by a solid line) vs. LiTFSI-doped PEO (hollow triangles) and LiTFSI-doped POEM (hollow circles) obtained from ref. 123; t_{Li^+} was obtained from ref. 49). The error bars (most of which are smaller than the data points) represent the standard deviations from averaging the 5-min and 8-min impedance measurements.

The highest ionic conductivities were obtained in the blend system consisting of 52 kg/mol PLiMTFSI and 5.9 kg/mol POEM at $r = 10:1$, with overall conductivities comparable to both LiTFSI-doped POEM and PEO (**Figure 2c**). The t_{Li^+} of this blend electrolyte was determined from potentiostatic polarization (using the current response before and after cell polarization; see **Figure S15**, **Table S4**, and associated text) and AC impedance spectroscopy (using the impedance response; see **Figures S16 – S19**, **Table S4**, and associated text). A value close to unity ($t_{\text{Li}^+} \approx 0.9$) was obtained for all cells due to the immobilized anion.^{1,4,5,124-128} The Li^+ conductivities were calculated by multiplying the overall conductivities by t_{Li^+} . As shown in **Figure 2d**, the Li^+ conductivities of PLiMTFSI – 52 / POEM were significantly higher than the LiTFSI-doped POEM and PEO systems across a broad temperature range. Thus, PLiMTFSI – 52 / POEM simultaneously imparted both high ionic conductivities and high Li^+ selectivities, which suggests that the polymer packing frustration is a powerful tool for developing all-solid-state SIC SPEs with improved performance.

To quantify the ion transport efficiency, the angular-frequency-dependent conductivity data (from both the 5-min and 8-min impedance measurements) were fit by the Jonscher Power Law to estimate ion hopping times (**Figure 3a**). The Jonscher Power Law equation describes the relaxation phenomena of the ionic environment arising from the hopping of mobile charge carriers (eq 5),^{129,130}

$$\sigma_{\text{AC}} = \sigma_0 + A\omega^n, \quad (5)$$

in which σ_{AC} is the AC conductivity, σ_0 is the direct current conductivity, A is the strength of polarizability, ω is the angular frequency of the sinusoidal voltage applied to the cell, and n is the dimensionless frequency exponent representing the interaction between mobile ions and surrounding lattice.^{131,132} For blend electrolytes displaying Arrhenius-like conductivities, the ion hopping time (τ) can be calculated from eq 6,¹³¹

$$\tau = \frac{2\pi}{\left(\frac{\sigma_0}{A}\right)^{\frac{1}{n}}}. \quad (6)$$

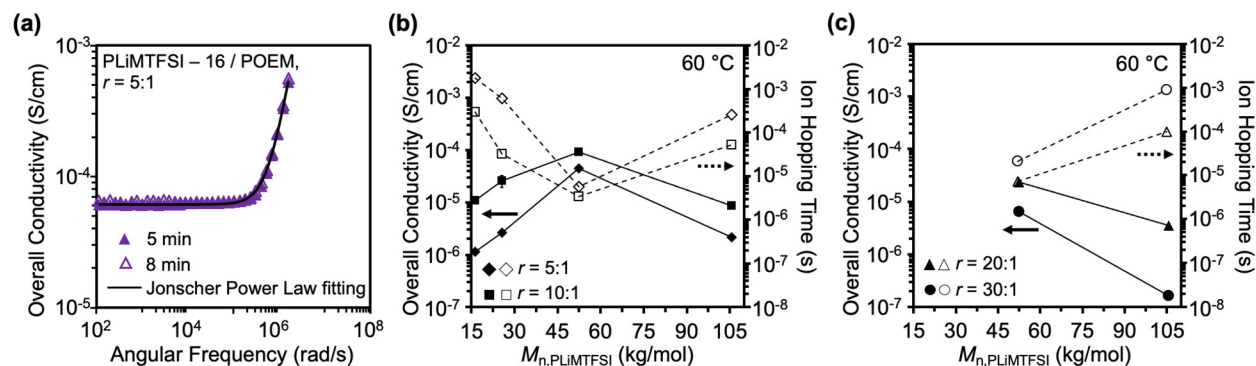


Figure 3. (a) Ionic conductivities (data points) and fit (solid line) as a function of angular frequency for PLiMTFSI – 16 / POEM blend electrolyte ($r = 5:1$). Ionic conductivities (filled data points) and ion hopping times (hollow data points) as a function of $M_{n,PLiMTFSI}$ at 60 °C for (b) $r = 5:1$ and 10:1 and (c) $r = 20:1$ and 30:1. The results for 90 °C and 110 °C are located in **Figure S20** and **Table S6**. The lines between data points are to guide the eye. The error bars for the conductivity data in (b) and (c), most of which are smaller than the data points, represent the standard deviations from averaging the 5-min and 8-min impedance measurements.

τ has an inverse relationship with the conductivity, as higher conductivities correspond to shorter ion hopping times (**Figure 3b** and **Figure 3c**; the results for 90 °C and 110 °C are located in **Figure S20** and **Table S6**). As $M_{n,PLiMTFSI}$ increased from 16 kg/mol to 52 kg/mol, the conductivities of the blend electrolytes at 60 °C were enhanced by ~ 2 orders of magnitude for $r = 5:1$ (from $\sim 10^{-6}$ S/cm to $\sim 10^{-4}$ S/cm) and ~ 1 order of magnitude for $r = 10:1$ (from $\sim 10^{-5}$ S/cm to $\sim 10^{-4}$ S/cm), while τ had ~ 2 order-of-magnitude decrease for $r = 5:1$ (from $\sim 10^{-3}$ s to $\sim 10^{-5}$ s) and ~ 1 order-of-magnitude drop for $r = 10:1$ (from $\sim 10^{-4}$ s to $\sim 10^{-5}$ s) (**Figure 3b**). As $M_{n,PLiMTFSI}$ was increased further from 52 kg/mol to 105 kg/mol, the conductivities dropped, and correspondingly, an upturn in τ was found (**Figure 3b** and **Figure 3c**). The improved conductivities at intermediate $M_{n,PLiMTFSI}$ s could be attributed to increased packing frustration and more available sites with decreased distance between them; therefore, ions could more easily hop from one site to another, resulting in reduced τ .

Increasing $M_{n,PLiMTFSI}$ leads to stronger repulsive interactions that contribute to increased degree of packing frustration.

To quantify the effect of blend electrolyte composition on the degree of packing frustration, the thermal behavior of the neat PLiMTFSI and blend electrolytes was examined using DSC (see **Figures S7 – S11**, **Table S2**, and the associated text). As shown in **Figure 4a** and **Figure 4b**, the T_g of neat PLiMTFSI ($T_{g,PLiMTFSI}$) followed the Flory – Fox equation (eq 7),¹³³

$$T_{g,PLiMTFSI} = T_{g,\infty,PLiMTFSI} - \frac{K}{M_{n,PLiMTFSI}}, \quad (7)$$

in which $T_{g,\infty,PLiMTFSI}$ is $T_{g,PLiMTFSI}$ at infinite M_n , and K is an empirical parameter that is related to the free volume generated by polymer chain ends.¹³³ Using eq 7, the $T_{g,\infty,PLiMTFSI}$ was calculated to be 409 K (136 °C) – close to the T_g s of PLiMTFSI – 52 (132 °C) and PLiMTFSI – 105 (134 °C) –

suggesting that chain-end effects become almost negligible at the higher molecular weights (see the plateau in **Figure 4b**).

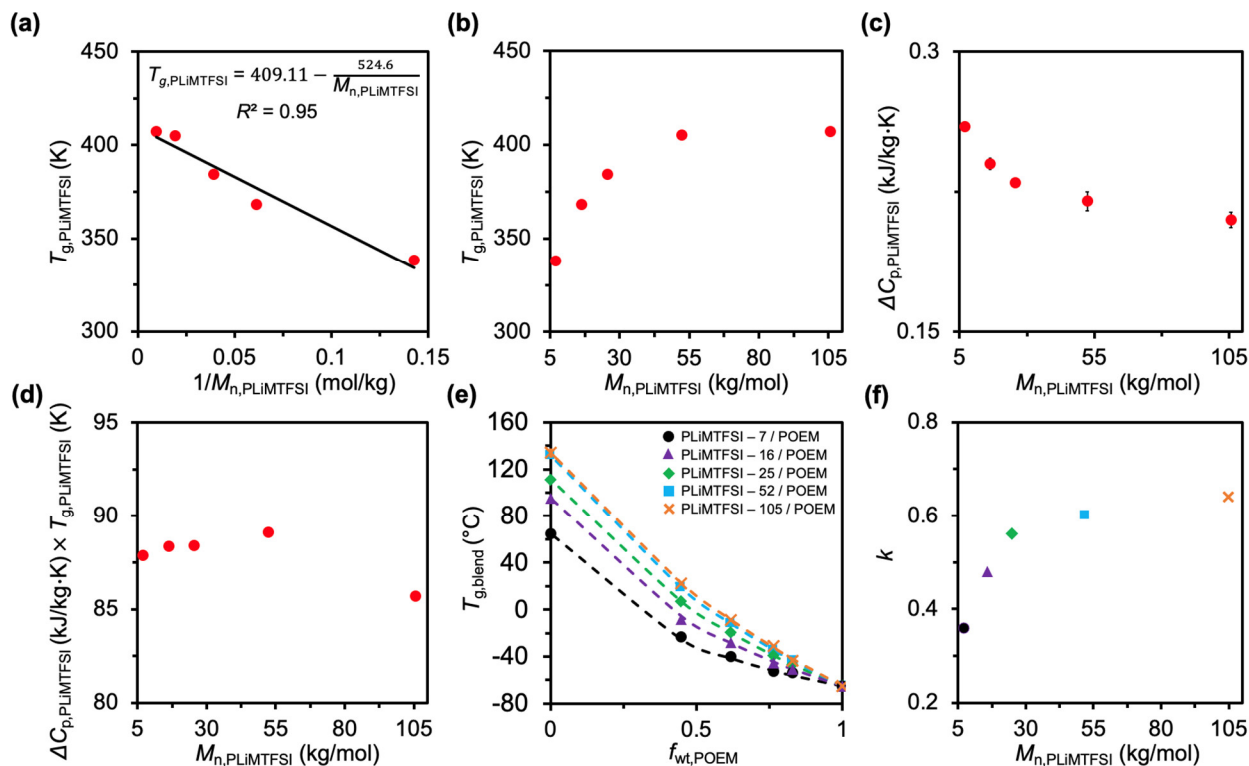


Figure 4. $T_{g,PLiMTFSI}$ plotted as a function of (a) $1/M_{n,PLiMTFSI}$ and (b) $M_{n,PLiMTFSI}$. Fit to the Fox-Flory equation shown as the solid line. (c) $\Delta C_{p,PLiMTFSI}$ and (d) $\Delta C_{p,PLiMTFSI} \times T_{g,PLiMTFSI}$ as a function of $M_{n,PLiMTFSI}$. (e) $T_{g,blend}$ (data points) and fits to Gordon – Taylor equation (dashed lines) for PLiMTFSI – 7 / POEM (black circles), PLiMTFSI – 16 / POEM blend electrolyte (purple triangles), PLiMTFSI – 25 / POEM (green diamonds), PLiMTFSI – 52 / POEM (blue squares), and PLiMTFSI – 105 / POEM (orange crosses) blend electrolytes. (f) Fitting parameter k as a function of $M_{n,PLiMTFSI}$. The error bars in (a), (b), (c), (d), and (e), most of which are smaller than the data points, represent the standard deviations from averaging the values obtained from the second and third DSC heating traces.

As shown in **Figure 4c**, the heat capacity change of PLiMTFSI at $T_{g,PLiMTFSI}$ ($\Delta C_{p,PLiMTFSI}$) is inversely related to $M_{n,PLiMTFSI}$. $\Delta C_{p,PLiMTFSI}$ represents the configurational variations (freedom) of the polymer at $T_{g,PLiMTFSI}$,⁹⁸ and initially decreased sharply with $M_{n,PLiMTFSI}$ from 7 kg/mol to 25 kg/mol, then began to plateau as $M_{n,PLiMTFSI}$ exceeded 25 kg/mol (*e.g.*, in the 52 and 105 kg/mol specimens). The $M_{n,PLiMTFSI}$ at which $\Delta C_{p,PLiMTFSI}$ becomes invariant is comparable to the value associated with $T_{g,\infty,PLiMTFSI}$. As the chains-end concentration decreases, less configurational freedom is conferred to the polymer.¹¹² Moreover, for 7, 16, 25, and 52 kg/mol specimens, $\Delta C_{p,PLiMTFSI}$ and $T_{g,PLiMTFSI}$ followed Boyer’s rule¹³⁴ (eq 8) (**Figure 4d**),

$$\Delta C_{p,PLiMTFSI} \times T_{g,PLiMTFSI} = \text{constant} . \quad (8)$$

A slight deviation from this simple relationship was seen in the 105 kg/mol specimen. This deviation has been reported for cases in which high- M_n rigid polymers are associated with higher vibrational contributions to ΔC_p .¹¹² The quantitatively similar behavior between M_n , PLiMTFSI-dependent $T_{g, \text{PLiMTFSI}}$ and $\Delta C_{p, \text{PLiMTFSI}}$ indicates that M_n , T_g , ΔC_p , free volume, and configurational freedom are all closely correlated with each other.

For the blend electrolytes, $T_{g, \text{blend}}$ (**Figure 4e**) could be fit to the Gordon – Taylor equation (eq 9),¹³⁵

$$T_{g, \text{blend}} = \frac{w_1 T_{g,1} + k w_2 T_{g,2}}{w_1 + k w_2}, \quad (9)$$

in which w_1 and w_2 are the weight fractions of each homopolymer component, POEM and PLiMTFSI, respectively, and $T_{g,1}$ and $T_{g,2}$ are the T_g values of neat POEM and PLiMTFSI, respectively.¹³⁵ The Gordon – Taylor equation describes the impact of composition and deviations from ideal mixing on polymer blend T_g ,¹³⁵ in which the adjustable fitting parameter k typically ranges between 0 and 1 and accounts for negative deviations from the ideal binary mixing.^{136,137} As shown in **Figure 4f**, k initially increased sharply with M_n , PLiMTFSI from 7 kg/mol to 25 kg/mol, then plateaued as M_n , PLiMTFSI exceeded 25 kg/mol (*e.g.*, in the 52 and 105 kg/mol specimens). This trend quantitatively mirrors the $T_{g, \text{PLiMTFSI}}$ and $\Delta C_{p, \text{PLiMTFSI}}$ behaviors as a function of molecular weight. It has been suggested that k is correlated with ΔC_p and/or free volume (re)distribution upon mixing, depending on whether eq 9 is derived from the configurational entropy theory¹³⁸ or the free volume theory.¹³⁹ k is also related to conformational energy barriers, contact between polymer components, and chain conformational (re)arrangement,^{136,138-141} detailed analysis could provide additional insight but is beyond the scope of this work. The M_n -dependence of k is in line with the literature, in which k increases are especially evident for the blends with lower- M_n (≤ 40 kg/mol) rigid component, and k is nearly constant for blends with higher M_n (> 40 kg/mol) rigid polymer.¹³⁶ In the 7, 16, and 25 kg/mol PLiMTFSI-containing specimens, the rapid change in k was attributed to stronger intermolecular interactions within the blend electrolyte,¹³⁵⁻¹³⁷ specifically the electrostatic repulsions between PLiMTFSI pendant groups and the steric repulsions between methyl groups (in both PLiMTFSI and POEM). When higher molecular-weight PLiMTFSI (52 and 105 kg/mol) was incorporated into the blend electrolytes, k nearly plateaued, likely due to the decreased chain-end effect illustrated by the $T_{g, \text{PLiMTFSI}}$ and $\Delta C_{p, \text{PLiMTFSI}}$ behaviors.

Thermodynamic and kinetic fragility are closely correlated to the molecular weight-based VTF to Arrhenius crossover.

To investigate blend electrolyte composition effects on the thermodynamic and kinetic fragility, DSC was used to determine both fragility values (see **Table S2** and the associated text). The thermodynamic fragility was expressed as ΔC_p .¹⁴² As shown in **Figure 5a**, ΔC_p decreased as the PLiMTFSI weight fraction increased, and this drop in ΔC_p could suggest stronger restrictions on molecular rearrangements within the electrolytes due to strengthened electrostatic repulsions (between PLiMTFSI pendant groups). The kinetic fragility m can be estimated from a straightforward relationship between m and T_g (eq 10) using the Williams–Landel–Ferry equation with C_1 (17.4) and C_2 (51.6 K),^{142,143}

$$m = \frac{C_1}{C_2} \times T_g \approx 0.34 T_g. \quad (10)$$

m is a measure of the packing frustration, in which larger values of m indicate that the system is more packing frustrated.^{90,104} As shown in **Figure 5b**, the kinetic fragility increased upon incorporating higher weight fractions of PLiMTFSI into the blend electrolyte, likely because the repulsive interactions between PLiMTFSI pendent groups become stronger, disfavoring efficient chain packing.

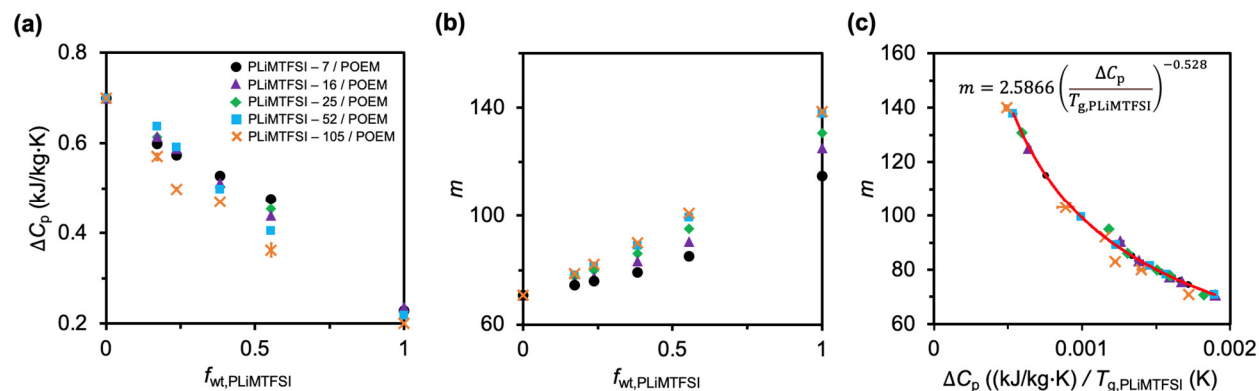


Figure 5. (a) ΔC_p and (b) m as a function of PLiMTFSI weight fraction for PLiMTFSI – 7 / POEM (black circles), PLiMTFSI – 16 / POEM (purple triangles), PLiMTFSI – 25 / POEM (green diamonds), PLiMTFSI – 52 / POEM (blue squares), and PLiMTFSI – 105 / POEM (orange crosses) blend electrolytes. (c) Correlation between m and ΔC_p . The red solid line represents the fit of the data points. The error bars (most of which are smaller than the data points) represent the standard deviations from averaging the values obtained from the second and third DSC heating traces.

The correlation between the thermodynamic and kinetic fragility of the blend electrolytes is shown in **Figure 5c**. The connection between the two fragility parameters enables the prediction of m . For rigid polymers, m is strongly dependent on M_n and ranges from ~ 80 to ~ 200 as M_n increases, whereas for flexible polymers, m is only weakly dependent on M_n and typically ranges from ~ 40 to ~ 80 as M_n increases.¹⁴⁴ Higher values of m suggest that ion transport is largely decoupled from the matrix segmental relaxation (Arrhenius-like ion hopping motion).^{90,104} This trend is in line with the ion transport transitions from VTF-like to Arrhenius-like (**Figure 1a-d**). However, it is difficult to find a generalized ‘cutoff’ value to distinguish VTF-like vs. Arrhenius-like ion transport. For instance, PLiMTFSI – 7 / POEM ($r = 5:1$) had a m of ~ 114 with VTF-like ion transport, while PLiMTFSI – 16 / POEM ($r = 5:1$) had a m of ~ 90 but with Arrhenius-like ion hopping. As mentioned previously, polymer molecular characteristics, architecture, chemistry, backbone / side group rigidity, and molecular interactions all contribute to the packing efficiency within polymer materials, a qualitative (or even quantitative) picture would provide significant insight into designing SPEs with superior ion transport properties.

Immobilized TFSI anion leads to comparable limiting current densities and enhanced electrochemical stabilities vs. PEO/LiTFSI.

The limiting current density was measured through a chronopotentiometry method on a lithium – lithium symmetric cell under increasing current densities from 0.8 mA/cm² to 1.9 mA/cm². The potential vs. time data are shown in **Figure 6a** and **Figure 6b**. The results for three

replicate cells are shown in **Figure S21**, and the potential responses were in good agreement across all cells. The measurement temperature for the limiting current density was chosen to be 60 °C to compare with literature data at similar temperatures to minimize any potential temperature impacts on the comparative results. The limiting current density of PLiMTFSI – 52 / POEM, $r = 10:1$ was 1.8 mA/cm², *i.e.*, the highest current density at which a steady-state potential was reached. The limiting current density of the SIC polymer blend electrolyte (1.8 mA/cm², electrolyte thickness, $L = 0.05$ cm) was comparable to the theoretical limiting current density of PEO/LiTFSI (~ 1.8 mA/cm², electrolyte thickness = 0.025 cm) at the same ion concentration¹⁴⁵ and surpassed that of a number of solvent-plasticized SIC polymers.¹⁴⁶⁻¹⁵⁰ Although the effect of the electrolyte thickness on the limiting current density has been well-established for dual-ion-conducting polymers, such a study is not commonly undertaken for SIC systems.^{52,60,145} Theoretically, limiting current densities in SIC polymers should be close to infinity as t_{Li^+} approaches 1 if one can neglect chain mobility (and thereby no anion mobility).^{60,151,152} Herein, in comparison to solvent-plasticized SIC systems, the enhanced limiting current density could be attributed to the high- M_n PLiMTFSI with bulky side groups and transient TFSI – Li⁺ – EO crosslinks at high ion concentrations ($r = 10:1$).¹⁰⁵⁻¹⁰⁷ Both features significantly reduce the ion mobility in this solid-state, SIC, polymer blend electrolyte.

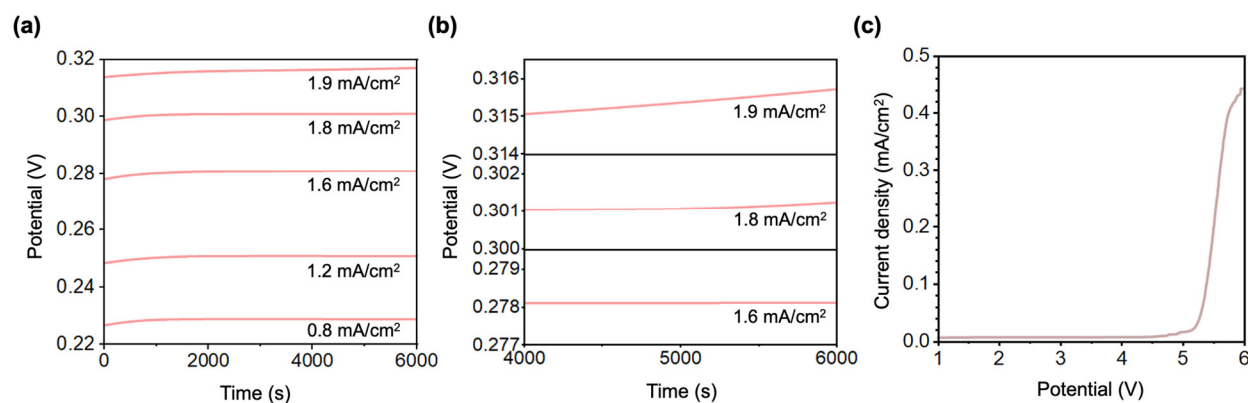


Figure 6. Potential vs. time under different current densities for PLiMTFSI – 52 / POEM, $r = 10:1$ blend electrolyte (thickness, $L = 0.05$ cm) of the (a) whole-time region and (b) 4000-6000 s region for an expanded view. (c) Current density vs. potential for PLiMTFSI – 52 / POEM, $r = 10:1$ blend electrolyte.

The electrochemical stability of the blend electrolyte was determined by linear sweep voltammetry on a lithium – stainless steel cell (**Figure 6c**). The results for three replicate cells are shown in **Figure S22**, and the current density responses were in good agreement among all the cells. In PLiMTFSI – 52 / POEM, $r = 10:1$ electrolyte, the current densities were below 0.01 mA/cm² in the 1.0 – 4.7 V voltage window, then increased rapidly above 4.7 V likely due to oxidation. This electrochemical stability was significantly enhanced in comparison to the benchmark PEO/LiTFSI (~ 3.5 V against Li⁺ / Li).⁵² Overall, these results demonstrate that restricting anion motion is an effective approach to realize improved performance in full SPEs.

Conclusions

This work demonstrates that a fully solid-state, single-ion-conducting, polymer blend electrolyte with improved ion transport can be achieved by overcoming the constraints of polymer segmental relaxation. The rigid PLiMTFSI with high M_n (52 kg/mol) led to significant chain packing frustration within the electrolyte at relatively high ion concentrations (*e.g.*, [EO]:[Li] = 10:1) and generated percolating free volume that served as interconnected Li^+ diffusion pathways. As the blend electrolyte became more packing frustrated with increasing $M_{n,\text{PLiMTFSI}}$ and ion concentration, the ion transport transitioned from being closely coupled to polymer segmental dynamics (VTF-like) to rapid and selective hopping (Arrhenius-like) across a broad temperature range (30 – 150 °C), well above $T_{g,\text{blend}}$. For example, the blend containing 52 kg/mol PLiMTFSI and 5.9 kg/mol POEM at $r = 10:1$ exhibited superior ionic conductivities ($\approx 7 \times 10^{-3}$ S/cm at 150 °C), Li^+ selectivities ($t_{\text{Li}^+} = 0.9$), electrochemical stabilities up to 4.7 V against Li^+ / Li , and limiting current densities of 1.8 mA/cm² (electrolyte thickness = 0.05 cm). These results suggest that this SIC polymer blend electrolyte might be a promising alternative to the benchmark PEO/LiTFSI system. Additionally, the polymer packing efficiency and corresponding thermal and conductive properties in these blends could be easily tuned by polymer molecular characteristics, such as molecular weight, and a correlation between thermodynamic and kinetic fragility was empirically determined to assist in assessing the temperature-dependent conduction behavior. Taken together, this SIC polymer blend electrolyte overcomes the trade-off between high t_{Li^+} and high ionic conductivity, highlighting the potential of decoupling ion transport from segmental relaxation, to generate SPEs with improved safety, energy efficiency, and output characteristics.

Associated Content

Supporting Information

Neat PLiMTFSI and neat POEM characterization *via* ¹H NMR spectroscopy, SEC, TGA, DSC, and DMA; blend electrolytes characterization *via* DSC and DMA; ionic conductivity vs. 1000/T, imaginary impedance vs. real impedance, and real impedance vs. AC frequency for one cell with aluminum blocking electrodes and three replicate cells with lithium non-blocking electrodes; impedance response before and after polarization *via* AC impedance spectroscopy for four lithium – lithium symmetric cells; current response before and after polarization *via* potentiostatic polarization for four lithium – lithium symmetric cells; initial current vs. time for the first 0.98s for four lithium – lithium symmetric cells; initial current comparison between Ohm's law calculation and direct measurements for four lithium – lithium symmetric cells; ion hopping time vs. $M_{n,\text{PLiMTFSI}}$ for blend electrolytes exhibiting Arrhenius conductivity behavior; potential vs. time for four lithium – lithium symmetric cells; steady-state potential response comparison between Ohm's law calculation and chronopotentiometry measurements for four lithium – lithium symmetric cells; current density vs. potential for four lithium – stainless steel cells

Author Information

Corresponding Author

Thomas H. Epps, III – *Department of Chemical & Biomolecular Engineering, University of Delaware, Newark, Delaware 19716, United States; Department of Materials Science & Engineering, University of Delaware, Newark, Delaware 19716, United States; and Center for Research in Soft matter & Polymers (CRiSP), University of Delaware, Newark, Delaware 19716, United States; orcid.org/0000-0002-2513-0966; Email: thepps@udel.edu*

Author

Mengying Yang – *Department of Materials Science & Engineering, University of Delaware, Newark, Delaware 19716, United States; orcid.org/0009-0008-1254-1599*

Acknowledgment

M.Y. and T.H.E. thank a Department of Energy grant (DOE BES; DE-SC0014458) for financial support. The authors also acknowledge the U.S. Department of Energy's Office of Energy Efficiency and Renewable Energy (EERE) for providing the funding under the Award Number DE-EE0009185 to support the limiting current density measurements. NMR spectroscopy was partially supported by the Delaware COBRE program, with a grant from the National Institute of General Medical Sciences–NIGMS (5 P30 GM110758-02) from the National Institutes of Health (NIH). The authors thank the UD Advanced Materials Characterization Lab for use of the DSC instrument, Prof. Laure V. Kayser for use of the SEC instrument, Prof. Michael E. Mackay for use of the rheometer, and Prof. Koffi Pierre Yao for providing the lithium foil electrodes. Certain commercial equipment, instruments, materials, suppliers, or software are identified in this paper to facilitate the understanding and interpretation of data. Such identifications do not imply recommendation or endorsement by DOE or NIH, nor do they imply that the materials or equipment identified are necessarily the best available for the purpose.

References

1. Morris, M. A.; An, H.; Lutkenhaus, J. L.; Epps, T. H., III, Harnessing the Power of Plastics: Nanostructured Polymer Systems in Lithium-Ion Batteries. *ACS Energy Letters* **2017**, *2* (8), 1919-1936.
2. Wheatle, B. K.; Keith, J. R.; Mogurampelly, S.; Lynd, N. A.; Ganesan, V., Influence of Dielectric Constant on Ionic Transport in Polyether-Based Electrolytes. *ACS Macro Letters* **2017**, *6* (12), 1362-1367.
3. Weber, R. L.; Mahanthappa, M. K., Thiol-ene synthesis and characterization of lithium bis(malonato)borate single-ion conducting gel polymer electrolytes. *Soft Matter* **2017**, *13* (41), 7633-7643.
4. Ketkar, P. M.; Shen, K.-H.; Hall, L. M.; Epps, T. H., III, Charging toward improved lithium-ion polymer electrolytes: exploiting synergistic experimental and computational approaches to facilitate materials design. *Molecular Systems Design & Engineering* **2019**, *4* (2), 223-238.
5. Diederichsen, K. M.; McShane, E. J.; McCloskey, B. D., Promising Routes to a High Li⁺ Transference Number Electrolyte for Lithium Ion Batteries. *ACS Energy Letters* **2017**, *2* (11), 2563-2575.
6. Young, W.-S.; Kuan, W.-F.; Epps, T. H., III, Block copolymer electrolytes for rechargeable lithium batteries. *Journal of Polymer Science Part B: Polymer Physics* **2014**, *52* (1), 1-16.
7. Dewing, B. L.; Bible, N. G.; Ellison, C. J.; Mahanthappa, M. K., Electrochemically Stable, High Transference Number Lithium Bis(malonato)borate Polymer Solution Electrolytes. *Chemistry of Materials* **2020**, *32* (9), 3794-3804.
8. Lamb, J.; Orendorff, C. J.; Roth, E. P.; Langendorf, J., Studies on the Thermal Breakdown of Common Li-Ion Battery Electrolyte Components. *Journal of The Electrochemical Society* **2015**, *162* (10), A2131-A2135.
9. Homann, G.; Stolz, L.; Nair, J.; Laskovic, I. C.; Winter, M.; Kasnatscheew, J., Poly(Ethylene Oxide)-based Electrolyte for Solid-State-Lithium-Batteries with High Voltage Positive Electrodes: Evaluating the Role of Electrolyte Oxidation in Rapid Cell Failure. *Scientific Reports* **2020**, *10* (1), 4390.
10. Snyder, R. L.; Choo, Y.; Gao, K. W.; Halat, D. M.; Abel, B. A.; Sundararaman, S.; Prendergast, D.; Reimer, J. A.; Balsara, N. P.; Coates, G. W., Improved Li⁺ Transport in Polyacetal Electrolytes: Conductivity and Current Fraction in a Series of Polymers. *ACS Energy Letters* **2021**, *6* (5), 1886-1891.
11. Kim, S. H.; Hong, K.; Xie, W.; Lee, K. H.; Zhang, S.; Lodge, T. P.; Frisbie, C. D., Electrolyte-gated transistors for organic and printed electronics. *Advanced Materials* **2013**, *25* (13), 1822-1846.
12. St-Onge, V.; Cui, M.; Rochon, S.; Daigle, J.-C.; Claverie, J. P., Reducing crystallinity in solid polymer electrolytes for lithium-metal batteries *via* statistical copolymerization. *Communications Materials* **2021**, *2* (1), 83.
13. Bannister, D. J.; Davies, G. R.; Ward, I. M.; McIntyre, J. E., Ionic conductivities of poly(methoxy polyethylene glycol monomethacrylate) complexes with LiSO₃CH₃. *Polymer* **1984**, *25* (11), 1600-1602.
14. Deng, C.; Webb, M. A.; Bennington, P.; Sharon, D.; Nealey, P. F.; Patel, S. N.; de Pablo, J. J., Role of Molecular Architecture on Ion Transport in Ethylene oxide-Based Polymer Electrolytes. *Macromolecules* **2021**, *54* (5), 2266-2276.

15. Rolland, J.; Brassinne, J.; Bourgeois, J. P.; Poggi, E.; Vlad, A.; Gohy, J. F., Chemically anchored liquid-PEO based block copolymer electrolytes for solid-state lithium-ion batteries. *Journal of Materials Chemistry A* **2014**, *2* (30), 11839-11846.
16. Morris, M. A.; Gartner, T. E., III; Epps, T. H., III, Tuning Block Polymer Structure, Properties, and Processability for the Design of Efficient Nanostructured Materials Systems. *Macromolecular Chemistry and Physics* **2017**, *218* (5), 1600513.
17. Kuan, W.-F.; Remy, R.; Mackay, M. E.; Epps, T. H., III, Controlled ionic conductivity via tapered block polymer electrolytes. *RSC Advances* **2015**, *5* (17), 12597-12604.
18. Luo, M.; Brown, J. R.; Remy, R. A.; Scott, D. M.; Mackay, M. E.; Hall, L. M.; Epps, T. H., III, Determination of Interfacial Mixing in Tapered Block Polymer Thin Films: Experimental and Theoretical Investigations. *Macromolecules* **2016**, *49* (14), 5213-5222.
19. Ruzette, A.-V. G.; Soo, P. P.; Sadoway, D. R.; Mayes, A. M., Melt-Formable Block Copolymer Electrolytes for Lithium Rechargeable Batteries. *Journal of The Electrochemical Society* **2001**, *148* (6), A537-A543.
20. Sadoway, D. R., Block and graft copolymer electrolytes for high-performance, solid-state, lithium batteries. *Journal of Power Sources* **2004**, *129* (1), 1-3.
21. Patel, S. N.; Javier, A. E.; Beers, K. M.; Pople, J. A.; Ho, V.; Segalman, R. A.; Balsara, N. P., Morphology and Thermodynamic Properties of a Copolymer with an Electronically Conducting Block: Poly(3-ethylhexylthiophene)-block-poly(ethylene oxide). *Nano Letters* **2012**, *12* (9), 4901-4906.
22. Barteau, K. P.; Wolffs, M.; Lynd, N. A.; Fredrickson, G. H.; Kramer, E. J.; Hawker, C. J., Allyl Glycidyl Ether-Based Polymer Electrolytes for Room Temperature Lithium Batteries. *Macromolecules* **2013**, *46* (22), 8988-8994.
23. Geng, Z.; Schausser, N. S.; Lee, J.; Schmeller, R. P.; Barbon, S. M.; Segalman, R. A.; Lynd, N. A.; Hawker, C. J., Role of Side-Chain Architecture in Poly(ethylene oxide)-Based Copolymers. *Macromolecules* **2020**, *53* (12), 4960-4967.
24. Xu, H.; Mahanthappa, M. K., Ionic Conductivities of Broad Dispersity Lithium Salt-Doped Polystyrene/Poly(ethylene oxide) Triblock Polymers. *Macromolecules* **2021**, *54* (18), 8798-8809.
25. Kurian, M.; Galvin, M. E.; Trapa, P. E.; Sadoway, D. R.; Mayes, A. M., Single-ion conducting polymer-silicate nanocomposite electrolytes for lithium battery applications. *Electrochimica Acta* **2005**, *50* (10), 2125-2134.
26. Polu, A. R.; Rhee, H.-W., Effect of Organic-Inorganic Hybrid Nanoparticles (POSS-PEG(n = 4)) on Thermal, Mechanical, and Electrical Properties of PEO-Based Solid Polymer Electrolytes. *Advances in Polymer Technology* **2017**, *36* (2), 145-151.
27. Mirmira, P.; Fuschi, C.; Gillett, W.; Ma, P.; Zheng, J.; Hood, Z. D.; Amanchukwu, C. V., Nonconductive Polymers Enable Higher Ionic Conductivities and Suppress Reactivity in Hybrid Sulfide-Polymer Solid State Electrolytes. *ACS Applied Energy Materials* **2022**, *5* (7), 8900-8912.
28. Wong, D. H. C.; Vitale, A.; Devaux, D.; Taylor, A.; Pandya, A. A.; Hallinan, D. T.; Thelen, J. L.; Mecham, S. J.; Lux, S. F.; Lapidus, A. M.; Resnick, P. R.; Meyer, T. J.; Kostecky, R. M.; Balsara, N. P.; DeSimone, J. M., Phase Behavior and Electrochemical Characterization of Blends of Perfluoropolyether, Poly(ethylene glycol), and a Lithium Salt. *Chemistry of Materials* **2015**, *27* (2), 597-603.

29. Ben youcef, H.; Garcia-Calvo, O.; Lago, N.; Devaraj, S.; Armand, M., Cross-Linked Solid Polymer Electrolyte for All-Solid-State Rechargeable Lithium Batteries. *Electrochimica Acta* **2016**, *220*, 587-594.
30. Lehmann, M. L.; Yang, G.; Nanda, J.; Saito, T., Well-designed Crosslinked Polymer Electrolyte Enables High Ionic Conductivity and Enhanced Salt Solvation. *Journal of The Electrochemical Society* **2020**, *167* (7), 070539.
31. Fu, F.; Zheng, Y.; Jiang, N.; Liu, Y.; Sun, C.; Zhang, A.; Teng, H.; Sun, L.; Xie, H., A Dual-Salt PEO-based polymer electrolyte with Cross-Linked polymer network for High-Voltage lithium metal batteries. *Chemical Engineering Journal* **2022**, *450*, 137776.
32. Choi, U. H.; Colby, R. H., The Role of Solvating 12-Crown-4 Plasticizer on Dielectric Constant and Ion Conduction of Poly(ethylene oxide) Single-Ion Conductors. *Macromolecules* **2017**, *50* (14), 5582-5591.
33. Wang, B.; Wu, Y.; Zhuo, S.; Zhu, S.; Chen, Y.; Jiang, C.; Wang, C., Synergistic effect of organic plasticizer and lepidolite filler on polymer electrolytes for all-solid high-voltage Li-metal batteries. *Journal of Materials Chemistry A* **2020**, *8* (12), 5968-5974.
34. Sangeetha, M.; Mallikarjun, A.; Aparna, Y.; Reddy, M. V.; Kumar, J. S. K.; Sreekanth, T. V. M.; Reddy, M. J., Dielectric studies and AC conductivity of PVDF-HFP: LiBF₄: EC plasticized polymer electrolytes. *Materials Today: Proceedings* **2021**, *44*, 2168-2172.
35. Dehghani, E.; Salami-Kalajahi, M.; Moghaddam, A. R.; Roghani-Mamaqani, H., In Situ Dendrimer-Crosslinked Gel Polymer Electrolytes for Lithium-Ion Batteries with High Ionic Conductivity and Excellent Electrochemical Performance. *ACS Applied Polymer Materials* **2022**, *4* (6), 4154-4165.
36. Li, Z.; Liu, Y.; Liang, X.; Yu, M.; Liu, B.; Sun, Z.; Hu, W.; Zhu, G., A single-ion gel polymer electrolyte based on polyimide grafted with lithium 3-chloropropanesulfonyl (trifluoromethanesulfonyl) imide for high performance lithium ion batteries. *Journal of Materials Chemistry A* **2023**, *11* (4), 1766-1773.
37. Kim, K. M.; Ly, N. V.; Won, J. H.; Lee, Y.-G.; Cho, W. I.; Ko, J. M.; Kaner, R. B., Improvement of lithium-ion battery performance at low temperature by adopting polydimethylsiloxane-based electrolyte additives. *Electrochimica Acta* **2014**, *136*, 182-188.
38. Grewal, M. S.; Tanaka, M.; Kawakami, H., Fabrication and characterizations of soft and flexible Poly(dimethylsiloxane)-incorporated network polymer electrolyte membranes. *Polymer* **2020**, *186*, 122045.
39. Zhao, S.; Zhang, Y.; Pham, H.; Carrillo, J.-M. Y.; Sumpter, B. G.; Nanda, J.; Dudney, N. J.; Saito, T.; Sokolov, A. P.; Cao, P.-F., Improved Single-Ion Conductivity of Polymer Electrolyte via Accelerated Segmental Dynamics. *ACS Applied Energy Materials* **2020**, *3* (12), 12540-12548.
40. Schausser, N. S.; Nikolaev, A.; Richardson, P. M.; Xie, S.; Johnson, K.; Susca, E. M.; Wang, H.; Seshadri, R.; Clément, R. J.; Read de Alaniz, J.; Segalman, R. A., Glass Transition Temperature and Ion Binding Determine Conductivity and Lithium-Ion Transport in Polymer Electrolytes. *ACS Macro Letters* **2021**, *10* (1), 104-109.
41. Amanchukwu, C. V.; Gunnarsdóttir, A. B.; Choudhury, S.; Newlove, T. L.; Magusin, P. C. M. M.; Bao, Z.; Grey, C. P., Understanding Lithium-Ion Dynamics in Single-Ion and Salt-in-Polymer Perfluoropolyethers and Polyethyleneglycol Electrolytes Using Solid-State NMR. *Macromolecules* **2023**, *56* (10), 3650-3659.

42. Ma, P.; Mirmira, P.; Amanchukwu, C. V., Effect of Building Block Connectivity and Ion Solvation on Electrochemical Stability and Ionic Conductivity in Novel Fluoroether Electrolytes. *ACS Central Science* **2021**, *7* (7), 1232-1244.
43. Tominaga, Y.; Shimomura, T.; Nakamura, M., Alternating copolymers of carbon dioxide with glycidyl ethers for novel ion-conductive polymer electrolytes. *Polymer* **2010**, *51* (19), 4295-4298.
44. Webb, M. A.; Jung, Y.; Pesko, D. M.; Savoie, B. M.; Yamamoto, U.; Coates, G. W.; Balsara, N. P.; Wang, Z.-G.; Miller, T. F., III, Systematic Computational and Experimental Investigation of Lithium-Ion Transport Mechanisms in Polyester-Based Polymer Electrolytes. *ACS Central Science* **2015**, *1* (4), 198-205.
45. Webb, M. A.; Savoie, B. M.; Wang, Z.-G.; Miller, T. F., III, Chemically Specific Dynamic Bond Percolation Model for Ion Transport in Polymer Electrolytes. *Macromolecules* **2015**, *48* (19), 7346-7358.
46. Pesko, D. M.; Webb, M. A.; Jung, Y.; Zheng, Q.; Miller, T. F., III; Coates, G. W.; Balsara, N. P., Universal Relationship between Conductivity and Solvation-Site Connectivity in Ether-Based Polymer Electrolytes. *Macromolecules* **2016**, *49* (14), 5244-5255.
47. Zheng, Q.; Pesko, D. M.; Savoie, B. M.; Timachova, K.; Hasan, A. L.; Smith, M. C.; Miller, T. F., III; Coates, G. W.; Balsara, N. P., Optimizing Ion Transport in Polyether-Based Electrolytes for Lithium Batteries. *Macromolecules* **2018**, *51* (8), 2847-2858.
48. Hiller, M. M.; Joost, M.; Gores, H. J.; Passerini, S.; Wiemhöfer, H. D., The influence of interface polarization on the determination of lithium transference numbers of salt in polyethylene oxide electrolytes. *Electrochimica Acta* **2013**, *114*, 21-29.
49. Chintapalli, M.; Timachova, K.; Olson, K. R.; Mecham, S. J.; Devaux, D.; DeSimone, J. M.; Balsara, N. P., Relationship between Conductivity, Ion Diffusion, and Transference Number in Perfluoropolyether Electrolytes. *Macromolecules* **2016**, *49* (9), 3508-3515.
50. Huo, S.; Sheng, L.; Xue, W.; Wang, L.; Xu, H.; Zhang, H.; He, X., Challenges of polymer electrolyte with wide electrochemical window for high energy solid-state lithium batteries. *InfoMat* **2023**, *5* (3), e12394.
51. Gregory, G. L.; Gao, H.; Liu, B.; Gao, X.; Rees, G. J.; Pasta, M.; Bruce, P. G.; Williams, C. K., Buffering Volume Change in Solid-State Battery Composite Cathodes with CO₂-Derived Block Polycarbonate Ethers. *Journal of the American Chemical Society* **2022**, *144* (38), 17477-17486.
52. Yu, X.; Hoffman, Z. J.; Lee, J.; Fang, C.; Gido, L. A.; Patel, V.; Eitouni, H. B.; Wang, R.; Balsara, N. P., A Practical Polymer Electrolyte for Lithium and Sodium Batteries: Poly(pentyl malonate). *ACS Energy Letters* **2022**, *7* (11), 3791-3797.
53. Benabed, Y.; Rioux, M.; Rousselot, S.; Hautier, G.; Dollé, M., Assessing the Electrochemical Stability Window of NASICON-Type Solid Electrolytes. *Frontiers in Energy Research* **2021**, *9*, 682008.
54. Zhou, W.; Wang, Z.; Pu, Y.; Li, Y.; Xin, S.; Li, X.; Chen, J.; Goodenough, J. B., Double-Layer Polymer Electrolyte for High-Voltage All-Solid-State Rechargeable Batteries. *Advanced Materials* **2019**, *31* (4), 1805574.
55. Vélez, J. F.; Aparicio, M.; Mosa, J., Covalent silica-PEO-LiTFSI hybrid solid electrolytes via sol-gel for Li-ion battery applications. *Electrochimica Acta* **2016**, *213*, 831-841.
56. Fang, R.; Xu, B.; Grundish, N. S.; Xia, Y.; Li, Y.; Lu, C.; Liu, Y.; Wu, N.; Goodenough, J. B., Li₂S₆-Integrated PEO-Based Polymer Electrolytes for All-Solid-State Lithium-Metal Batteries. *Angewandte Chemie International Edition* **2021**, *60* (32), 17701-17706.

57. Yang, Q.; Huang, J.; Li, Y.; Wang, Y.; Qiu, J.; Zhang, J.; Yu, H.; Yu, X.; Li, H.; Chen, L., Surface-protected LiCoO₂ with ultrathin solid oxide electrolyte film for high-voltage lithium ion batteries and lithium polymer batteries. *Journal of Power Sources* **2018**, *388*, 65-70.
58. Yang, X.; Jiang, M.; Gao, X.; Bao, D.; Sun, Q.; Holmes, N.; Duan, H.; Mukherjee, S.; Adair, K.; Zhao, C.; Liang, J.; Li, W.; Li, J.; Liu, Y.; Huang, H.; Zhang, L.; Lu, S.; Lu, Q.; Li, R.; Singh, C. V.; Sun, X., Determining the limiting factor of the electrochemical stability window for PEO-based solid polymer electrolytes: main chain or terminal –OH group? *Energy & Environmental Science* **2020**, *13* (5), 1318-1325.
59. Stolz, L.; Hochstädt, S.; Röser, S.; Hansen, M. R.; Winter, M.; Kasnatscheew, J., Single-Ion versus Dual-Ion Conducting Electrolytes: The Relevance of Concentration Polarization in Solid-State Batteries. *ACS Applied Materials & Interfaces* **2022**, *14* (9), 11559-11566.
60. Hoffman, Z. J.; Ho, A. S.; Chakraborty, S.; Balsara, N. P., Limiting Current Density in Single-Ion-Conducting and Conventional Block Copolymer Electrolytes. *Journal of The Electrochemical Society* **2022**, *169* (4), 043502.
61. Yan, L.; Rank, C.; Mecking, S.; Winey, K. I., Gyroid and Other Ordered Morphologies in Single-Ion Conducting Polymers and Their Impact on Ion Conductivity. *Journal of the American Chemical Society* **2020**, *142* (2), 857-866.
62. Paren, B. A.; Nguyen, N.; Ballance, V.; Hallinan, D. T.; Kennemur, J. G.; Winey, K. I., Superionic Li-Ion Transport in a Single-Ion Conducting Polymer Blend Electrolyte. *Macromolecules* **2022**, *55* (11), 4692-4702.
63. Fragiadakis, D.; Dou, S.; Colby, R. H.; Runt, J., Molecular mobility and Li⁺ conduction in polyester copolymer ionomers based on poly(ethylene oxide). *The Journal of Chemical Physics* **2009**, *130* (6), 064907.
64. Meziane, R.; Bonnet, J.-P.; Courty, M.; Djellab, K.; Armand, M., Single-ion polymer electrolytes based on a delocalized polyanion for lithium batteries. *Electrochimica Acta* **2011**, *57*, 14-19.
65. Feng, S.; Shi, D.; Liu, F.; Zheng, L.; Nie, J.; Feng, W.; Huang, X.; Armand, M.; Zhou, Z., Single lithium-ion conducting polymer electrolytes based on poly[(4-styrenesulfonyl)(trifluoromethanesulfonyl)imide] anions. *Electrochimica Acta* **2013**, *93*, 254-263.
66. Dreier, P.; Pipertzis, A.; Spyridakou, M.; Mathes, R.; Floudas, G.; Frey, H., Introduction of Trifluoromethanesulfonamide Groups in Poly(ethylene oxide): Ionic Conductivity of Single-Ion-Conducting Block Copolymer Electrolytes. *Macromolecules* **2022**, *55* (4), 1342-1353.
67. Ding, Y.; Shen, X.; Zeng, J.; Wang, X.; Peng, L.; Zhang, P.; Zhao, J., Pre-irradiation grafted single lithium-ion conducting polymer electrolyte based on poly(vinylidene fluoride). *Solid State Ionics* **2018**, *323*, 16-24.
68. Cao, C.; Li, Y.; Feng, Y.; Long, P.; An, H.; Qin, C.; Han, J.; Li, S.; Feng, W., A sulfonimide-based alternating copolymer as a single-ion polymer electrolyte for high-performance lithium-ion batteries. *Journal of Materials Chemistry A* **2017**, *5* (43), 22519-22526.
69. Olmedo-Martínez, J. L.; Fdz De Anastro, A.; Martínez-Ibañez, M.; Müller, A. J.; Mecerreyes, D., Polyethylene Oxide/Sodium Sulfonamide Polymethacrylate Blends as Highly Conducting Single-Ion Solid Polymer Electrolytes. *Energy & Fuels* **2023**, *37* (7), 5519-5529.
70. Koseki, Y.; Aimi, K.; Ando, S., Crystalline structure and molecular mobility of PVDF chains in PVDF/PMMA blend films analyzed by solid-state ¹⁹F MAS NMR spectroscopy. *Polymer Journal* **2012**, *44* (8), 757-763.

71. Diederichsen, K. M.; Buss, H. G.; McCloskey, B. D., The Compensation Effect in the Vogel–Tammann–Fulcher (VTF) Equation for Polymer-Based Electrolytes. *Macromolecules* **2017**, *50* (10), 3831-3840.
72. Porcarelli, L.; Shaplov, A. S.; Bella, F.; Nair, J. R.; Mecerreyes, D.; Gerbaldi, C., Single-Ion Conducting Polymer Electrolytes for Lithium Metal Polymer Batteries that Operate at Ambient Temperature. *ACS Energy Letters* **2016**, *1* (4), 678-682.
73. Cheng, H.; Yan, C.; Orenstein, R.; Dirican, M.; Wei, S.; Subjalearndee, N.; Zhang, X., Polyacrylonitrile Nanofiber-Reinforced Flexible Single-Ion Conducting Polymer Electrolyte for High-Performance, Room-Temperature All-Solid-State Li-Metal Batteries. *Advanced Fiber Materials* **2022**, *4* (3), 532-546.
74. Liang, H.-P.; Zarrabeitia, M.; Chen, Z.; Jovanovic, S.; Merz, S.; Granwehr, J.; Passerini, S.; Bresser, D., Polysiloxane-Based Single-Ion Conducting Polymer Blend Electrolyte Comprising Small-Molecule Organic Carbonates for High-Energy and High-Power Lithium-Metal Batteries. *Advanced Energy Materials* **2022**, *12* (16), 2200013.
75. Dong, X.; Mayer, A.; Liu, X.; Passerini, S.; Bresser, D., Single-Ion Conducting Multi-block Copolymer Electrolyte for Lithium-Metal Batteries with High Mass Loading NCM₈₁₁ Cathodes. *ACS Energy Letters* **2023**, *8* (2), 1114-1121.
76. Riggleman, R. A.; Douglas, J. F.; de Pablo, J. J., Antiplasticization and the elastic properties of glass-forming polymer liquids. *Soft Matter* **2010**, *6* (2), 292-304.
77. Wang, Y.; Fan, F.; Agapov, A. L.; Saito, T.; Yang, J.; Yu, X.; Hong, K.; Mays, J.; Sokolov, A. P., Examination of the fundamental relation between ionic transport and segmental relaxation in polymer electrolytes. *Polymer* **2014**, *55* (16), 4067-4076.
78. Zhu, Y. S.; Wang, X. J.; Hou, Y. Y.; Gao, X. W.; Liu, L. L.; Wu, Y. P.; Shimizu, M., A new single-ion polymer electrolyte based on polyvinyl alcohol for lithium ion batteries. *Electrochimica Acta* **2013**, *87*, 113-118.
79. Borzutzki, K.; Thienenkamp, J.; Diehl, M.; Winter, M.; Brunklaus, G., Fluorinated polysulfonamide based single ion conducting room temperature applicable gel-type polymer electrolytes for lithium ion batteries. *Journal of Materials Chemistry A* **2019**, *7* (1), 188-201.
80. Zhang, S.; Dou, S.; Colby, R. H.; Runt, J., Glass transition and ionic conduction in plasticized and doped ionomers. *Journal of Non-Crystalline Solids* **2005**, *351* (33), 2825-2830.
81. Kadulkar, S.; Brotherton, Z. W.; Lynch, A. L.; Pohlman, G.; Zhang, Z.; Torres, R.; Manthiram, A.; Lynd, N. A.; Truskett, T. M.; Ganesan, V., The Importance of Morphology on Ion Transport in Single-Ion, Comb-Branched Copolymer Electrolytes: Experiments and Simulations. *Macromolecules* **2023**, *56* (7), 2790-2800.
82. Jones, S. D.; Nguyen, H.; Richardson, P. M.; Chen, Y.-Q.; Wyckoff, K. E.; Hawker, C. J.; Clément, R. J.; Fredrickson, G. H.; Segalman, R. A., Design of Polymeric Zwitterionic Solid Electrolytes with Superionic Lithium Transport. *ACS Central Science* **2022**, *8* (2), 169-175.
83. D'Angelo, A. J.; Panzer, M. J., Design of Stretchable and Self-Healing Gel Electrolytes via Fully Zwitterionic Polymer Networks in Solvate Ionic Liquids for Li-Based Batteries. *Chemistry of Materials* **2019**, *31* (8), 2913-2922.
84. Wieck, K. W.; Panzer, M. J., Ionogel Electrolytes Supported by Zwitterionic Copolymers Featuring Lithium Ion-Mediated, Noncovalent Cross-Links. *ACS Applied Polymer Materials* **2023**, *5* (4), 2887-2894.
85. Račko, D.; Capponi, S.; Alvarez, F.; Colmenero, J.; Bartoš, J., The free-volume structure of a polymer melt, poly(vinyl methylether) from molecular dynamics simulations and cavity analysis. *The Journal of Chemical Physics* **2009**, *131* (6), 064903.

86. Agapov, A. L.; Sokolov, A. P., Decoupling Ionic Conductivity from Structural Relaxation: A Way to Solid Polymer Electrolytes? *Macromolecules* **2011**, *44* (11), 4410-4414.
87. Budd, P. M.; McKeown, N. B.; Fritsch, D., Free volume and intrinsic microporosity in polymers. *Journal of Materials Chemistry* **2005**, *15* (20), 1977-1986.
88. Wojnarowska, Z.; Feng, H.; Fu, Y.; Cheng, S.; Carroll, B.; Kumar, R.; Novikov, V. N.; Kisliuk, A. M.; Saito, T.; Kang, N.-G.; Mays, J. W.; Sokolov, A. P.; Bocharova, V., Effect of Chain Rigidity on the Decoupling of Ion Motion from Segmental Relaxation in Polymerized Ionic Liquids: Ambient and Elevated Pressure Studies. *Macromolecules* **2017**, *50* (17), 6710-6721.
89. Fan, F.; Wang, Y.; Hong, T.; Heres, M. F.; Saito, T.; Sokolov, A. P., Ion Conduction in Polymerized Ionic Liquids with Different Pendant Groups. *Macromolecules* **2015**, *48* (13), 4461-4470.
90. Fan, F.; Wang, W.; Holt, A. P.; Feng, H.; Uhrig, D.; Lu, X.; Hong, T.; Wang, Y.; Kang, N.-G.; Mays, J.; Sokolov, A. P., Effect of Molecular Weight on the Ion Transport Mechanism in Polymerized Ionic Liquids. *Macromolecules* **2016**, *49* (12), 4557-4570.
91. Gawu, S. K.; Fourie, A., Assessment of the modified slump test as a measure of the yield stress of high-density thickened tailings. *Canadian Geotechnical Journal* **2004**, *41* (1), 39-47.
92. Singh, M.; Odusanya, O.; Wilmes, G. M.; Eitouni, H. B.; Gomez, E. D.; Patel, A. J.; Chen, V. L.; Park, M. J.; Fragouli, P.; Iatrou, H.; Hadjichristidis, N.; Cookson, D.; Balsara, N. P., Effect of Molecular Weight on the Mechanical and Electrical Properties of Block Copolymer Electrolytes. *Macromolecules* **2007**, *40* (13), 4578-4585.
93. Menard, K. P., *Dynamic Mechanical Analysis: A Practical Introduction*. 2nd ed.; Boca Raton, FL, USA, 2008.
94. Maccallum, J. R., Vincent, C. A., Eds.; *Polymer electrolyte reviews - 1*. Elsevier Applied Science: New York, 1987; Vol. 1.
95. Galluzzo, M. D.; Maslyn, J. A.; Shah, D. B.; Balsara, N. P., Ohm's law for ion conduction in lithium and beyond-lithium battery electrolytes. *The Journal of Chemical Physics* **2019**, *151* (2), 020901.
96. Evans, J.; Vincent, C. A.; Bruce, P. G., Electrochemical measurement of transference numbers in polymer electrolytes. *Polymer* **1987**, *28* (13), 2324-2328.
97. Loyens, W.; Maurer, F. H. J.; Jannasch, P., Melt-compounded salt-containing poly(ethylene oxide)/clay nanocomposites for polymer electrolyte membranes. *Polymer* **2005**, *46* (18), 7334-7345.
98. Hiemenz, P. C.; Lodge, T. P., *Polymer chemistry*. 2nd ed.; CRC press: Boca Raton, Florida, 2007.
99. Seki, S.; Susan, M. A. B. H.; Kaneko, T.; Tokuda, H.; Noda, A.; Watanabe, M., Distinct Difference in Ionic Transport Behavior in Polymer Electrolytes Depending on the Matrix Polymers and Incorporated Salts. *The Journal of Physical Chemistry B* **2005**, *109* (9), 3886-3892.
100. Chintapalli, M.; Le, T. N. P.; Venkatesan, N. R.; Mackay, N. G.; Rojas, A. A.; Thelen, J. L.; Chen, X. C.; Devaux, D.; Balsara, N. P., Structure and Ionic Conductivity of Polystyrene-block-poly(ethylene oxide) Electrolytes in the High Salt Concentration Limit. *Macromolecules* **2016**, *49* (5), 1770-1780.
101. Bates, C. M.; Chang, A. B.; Momčilović, N.; Jones, S. C.; Grubbs, R. H., ABA Triblock Brush Polymers: Synthesis, Self-Assembly, Conductivity, and Rheological Properties. *Macromolecules* **2015**, *48* (14), 4967-4973.

102. Young, W.-S.; Epps, T. H., III, Ionic Conductivities of Block Copolymer Electrolytes with Various Conducting Pathways: Sample Preparation and Processing Considerations. *Macromolecules* **2012**, *45* (11), 4689-4697.
103. Petrowsky, M.; Frech, R., Temperature Dependence of Ion Transport: The Compensated Arrhenius Equation. *The Journal of Physical Chemistry B* **2009**, *113* (17), 5996-6000.
104. Jones, S. D.; Bamford, J.; Fredrickson, G. H.; Segalman, R. A., Decoupling Ion Transport and Matrix Dynamics to Make High Performance Solid Polymer Electrolytes. *ACS Polymers Au* **2022** *2* (6), 430-448.
105. Xie, S.; Zhang, B.; Mao, Y.; He, L.; Hong, K.; Bates, F. S.; Lodge, T. P., Influence of Added Salt on Chain Conformations in Poly(ethylene oxide) Melts: SANS Analysis with Complications. *Macromolecules* **2020**, *53* (16), 7141-7149.
106. Loo, W. S.; Fang, C.; Balsara, N. P.; Wang, R., Uncovering Local Correlations in Polymer Electrolytes by X-ray Scattering and Molecular Dynamics Simulations. *Macromolecules* **2021**, *54* (14), 6639-6648.
107. Sharon, D.; Bennington, P.; Webb, M. A.; Deng, C.; de Pablo, J. J.; Patel, S. N.; Nealey, P. F., Molecular Level Differences in Ionic Solvation and Transport Behavior in Ethylene Oxide-Based Homopolymer and Block Copolymer Electrolytes. *Journal of the American Chemical Society* **2021**, *143* (8), 3180-3190.
108. Hoffman, D. J.; Fica-Contreras, S. M.; Fayer, M. D., Amorphous polymer dynamics and free volume element size distributions from ultrafast IR spectroscopy. *Proceedings of the National Academy of Sciences* **2020**, *117* (25), 13949-13958.
109. Lee, S.; Mattice, W. L., A “phantom bubble” model for the distribution of free volume in polymers. *Computational and Theoretical Polymer Science* **1999**, *9* (1), 57-61.
110. Druger, S. D.; Ratner, M. A.; Nitzan, A., Polymeric solid electrolytes: Dynamic bond percolation and free volume models for diffusion. *Solid State Ionics* **1983**, *9-10*, 1115-1120.
111. Ding, Y.; Novikov, V. N.; Sokolov, A. P.; Dalle-Ferrier, C.; Alba-Simionesco, C.; Frick, B., Influence of Molecular Weight on Fast Dynamics and Fragility of Polymers. *Macromolecules* **2004**, *37* (24), 9264-9272.
112. Santangelo, P. G.; Roland, C. M., Molecular Weight Dependence of Fragility in Polystyrene. *Macromolecules* **1998**, *31* (14), 4581-4585.
113. Zhang, W.; Douglas, J. F.; Starr, F. W., How Dispersity from Step-Growth Polymerization Affects Polymer Dynamics from Coarse-Grained Molecular Simulations. *Macromolecules* **2022**, *55* (22), 9901-9907.
114. Somoza, M. M.; Sluch, M. I.; Berg, M. A., Torsional Relaxation and Friction on the Nanometer Length Scale: Comparison of Small-Molecule Rotation in Poly(dimethylsiloxane) and Poly(isobutylene). *Macromolecules* **2003**, *36* (8), 2721-2732.
115. Kunal, K.; Robertson, C. G.; Pawlus, S.; Hahn, S. F.; Sokolov, A. P., Role of Chemical Structure in Fragility of Polymers: A Qualitative Picture. *Macromolecules* **2008**, *41* (19), 7232-7238.
116. Dudowicz, J.; Freed, K. F.; Douglas, J. F., Fragility of glass-forming polymer liquids. *The Journal of Physical Chemistry B* **2005**, *109* (45), 21350-21356.
117. Erman, B.; Mark, J. E., *Structures and properties of rubberlike networks*. Oxford University Press: New York, New York, 1997.
118. Liu, C.; Liu, Z.; Yin, X.; Wu, G., Tuning the Dynamic Fragility of Acrylic Polymers by Small Molecules: The Interplay of Hydrogen Bonding Strength. *Macromolecules* **2015**, *48* (12), 4196-4206.

119. Zhang, L.; Marsiglio, J. A.; Lan, T.; Torkelson, J. M., Dramatic Tunability of the Glass Transition Temperature and Fragility of Low Molecular Weight Polystyrene by Initiator Fragments Located at Chain Ends. *Macromolecules* **2016**, *49* (6), 2387-2398.
120. Schweizer, K. S.; Saltzman, E. J., Theory of dynamic barriers, activated hopping, and the glass transition in polymer melts. *The Journal of Chemical Physics* **2004**, *121* (4), 1984-2000.
121. Clark, A.; Biswas, Y.; Taylor, M. E.; Asatekin, A.; Panzer, M. J.; Schick, C.; Cebe, P., Glass-Forming Ability of Polyzwitterions. *Macromolecules* **2021**, *54* (21), 10126-10134.
122. Casalini, R.; Roland, C. M., Scaling of the segmental relaxation times of polymers and its relation to the thermal expansivity. *Colloid and Polymer Science* **2004**, *283* (1), 107-110.
123. Bennington, P.; Deng, C.; Sharon, D.; Webb, M. A.; de Pablo, J. J.; Nealey, P. F.; Patel, S. N., Role of solvation site segmental dynamics on ion transport in ethylene-oxide based side-chain polymer electrolytes. *Journal of Materials Chemistry A* **2021**, *9* (15), 9937-9951.
124. Meabe, L.; Goujon, N.; Li, C.; Armand, M.; Forsyth, M.; Mecerreyes, D., Single-Ion Conducting Poly(Ethylene Oxide Carbonate) as Solid Polymer Electrolyte for Lithium Batteries. *Batteries & Supercaps* **2020**, *3* (1), 68-75.
125. Lingua, G.; Grysan, P.; Vlasov, P. S.; Verge, P.; Shaplov, A. S.; Gerbaldi, C., Unique Carbonate-Based Single Ion Conducting Block Copolymers Enabling High-Voltage, All-Solid-State Lithium Metal Batteries. *Macromolecules* **2021**, *54* (14), 6911-6924.
126. Doyle, M. L.; Fuller, T. F.; Newman, J., The importance of the lithium ion transference number in lithium/polymer cells. *Electrochimica Acta* **1994**, *39*, 2073-2081.
127. Sadoway, D. R.; Huang, B.; Trapa, P. E.; Soo, P. P.; Bannerjee, P.; Mayes, A. M., Self-doped block copolymer electrolytes for solid-state, rechargeable lithium batteries. *Journal of Power Sources* **2001**, *97-98*, 621-623.
128. Zhao, S.; Song, S.; Wang, Y.; Keum, J.; Zhu, J.; He, Y.; Sokolov, A. P.; Cao, P.-F., Unraveling the Role of Neutral Units for Single-Ion Conducting Polymer Electrolytes. *ACS Applied Materials & Interfaces* **2021**, *13* (43), 51525-51534.
129. Schröder, T. B.; Dyre, J. C., ac Hopping Conduction at Extreme Disorder Takes Place on the Percolating Cluster. *Physical Review Letters* **2008**, *101* (2), 025901.
130. Jonscher, A. K., The 'universal' dielectric response. *Nature* **1977**, *267* (5613), 673-679.
131. Almond, D. P.; Duncan, G. K.; West, A. R., The determination of hopping rates and carrier concentrations in ionic conductors by a new analysis of ac conductivity. *Solid State Ionics* **1983**, *8* (2), 159-164.
132. Clark, A. G.; Salcedo Montero, M.; Govinna, N. D.; Lounder, S. J.; Asatekin, A.; Cebe, P., Relaxation dynamics of blends of PVDF and zwitterionic copolymer by dielectric relaxation spectroscopy. *Journal of Polymer Science* **2020**, *58* (9), 1311-1324.
133. Fox, T. G., Jr.; Flory, P. J., Second-Order Transition Temperatures and Related Properties of Polystyrene. I. Influence of Molecular Weight. *Journal of Applied Physics* **2004**, *21* (6), 581-591.
134. Boyer, R. F., $\Delta C_p T_g$ and related quantities for high polymers. *Journal of Macromolecular Science, Part B* **1973**, *7* (3), 487-501.
135. Gordon, M.; Taylor, J. S., Ideal copolymers and the second-order transitions of synthetic rubbers. I. Non-crystalline copolymers. *Journal of Applied Chemistry* **1952**, *2* (9), 493-500.
136. Schneider, H. A., The Gordon-Taylor equation. Additivity and interaction in compatible polymer blends. *Die Makromolekulare Chemie* **1988**, *189* (8), 1941-1955.

137. Choi, U. H.; Liang, S.; O'Reilly, M. V.; Winey, K. I.; Runt, J.; Colby, R. H., Influence of Solvating Plasticizer on Ion Conduction of Polysiloxane Single-Ion Conductors. *Macromolecules* **2014**, *47* (9), 3145-3153.
138. Gibbs, J. H.; DiMarzio, E. A., Nature of the Glass Transition and the Glassy State. *The Journal of Chemical Physics* **2004**, *28* (3), 373-383.
139. Williams, M. L.; Landel, R. F.; Ferry, J. D., The Temperature Dependence of Relaxation Mechanisms in Amorphous Polymers and Other Glass-forming Liquids. *Journal of the American Chemical Society* **1955**, *77* (14), 3701-3707.
140. Brekner, M. J.; Schneider, H. A.; Cantow, H. J., Approach to the composition dependence of the glass transition temperature of compatible polymer blends: 1. *Polymer* **1988**, *29* (1), 78-85.
141. Schneider, H. A.; Rieger, J.; Penzel, E., The glass transition temperature of random copolymers: 2. Extension of the Gordon-Taylor equation for asymmetric T_g vs composition curves. *Polymer* **1997**, *38* (6), 1323-1337.
142. Qin, Q.; McKenna, G. B., Correlation between dynamic fragility and glass transition temperature for different classes of glass forming liquids. *Journal of Non-Crystalline Solids* **2006**, *352* (28), 2977-2985.
143. Ferry, J. D., *Viscoelastic properties of polymers*. 3rd ed.; John Wiley & Sons: New York, New York, 1980.
144. Sokolov, A. P.; Novikov, V. N.; Ding, Y., Why many polymers are so fragile. *Journal of Physics: Condensed Matter* **2007**, *19* (20), 205116.
145. Gribble, D. A.; Frenck, L.; Shah, D. B.; Maslyn, J. A.; Loo, W. S.; Mongcopa, K. I. S.; Pesko, D. M.; Balsara, N. P., Comparing Experimental Measurements of Limiting Current in Polymer Electrolytes with Theoretical Predictions. *Journal of The Electrochemical Society* **2019**, *166* (14), A3228.
146. Borzutzki, K.; Nair, J. R.; Winter, M.; Brunklaus, G., Does Cell Polarization Matter in Single-Ion Conducting Electrolytes? *ACS Applied Materials & Interfaces* **2022**, *14* (4), 5211-5222.
147. Nguyen, H.-D.; Kim, G.-T.; Shi, J.; Paillard, E.; Judeinstein, P.; Lyonard, S.; Bresser, D.; Iojoiu, C., Nanostructured multi-block copolymer single-ion conductors for safer high-performance lithium batteries. *Energy & Environmental Science* **2018**, *11* (11), 3298-3309.
148. Steinle, D.; Chen, Z.; Nguyen, H.-D.; Kuenzel, M.; Iojoiu, C.; Passerini, S.; Bresser, D., Single-ion conducting polymer electrolyte for $\text{Li}||\text{LiNi}_{10.6}\text{Mn}_{0.2}\text{Co}_{0.2}\text{O}_2$ batteries—impact of the anodic cutoff voltage and ambient temperature. *Journal of Solid State Electrochemistry* **2022**, *26* (1), 97-102.
149. Ford, H. O.; Park, B.; Jiang, J.; Seidler, M. E.; Schaefer, J. L., Enhanced Li^+ Conduction within Single-Ion Conducting Polymer Gel Electrolytes via Reduced Cation–Polymer Interaction. *ACS Materials Letters* **2020**, *2* (3), 272-279.
150. Liang, H.-P.; Chen, Z.; Dong, X.; Zinkevich, T.; Indris, S.; Passerini, S.; Bresser, D., Photo-Cross-Linked Single-Ion Conducting Polymer Electrolyte for Lithium-Metal Batteries. *Macromolecular Rapid Communications* **2022**, *43* (12), 2100820.
151. Chazalviel, J. N., Electrochemical aspects of the generation of ramified metallic electrodeposits. *Physical Review A* **1990**, *42* (12), 7355-7367.
152. Brissot, C.; Rosso, M.; Chazalviel, J. N.; Lascaud, S., In Situ Concentration Cartography in the Neighborhood of Dendrites Growing in Lithium/Polymer-Electrolyte/Lithium Cells. *Journal of The Electrochemical Society* **1999**, *146* (12), 4393-4400.

For Table of Contents Only

